Journal of Medicinal Chemistry

ARTICLE

pubs.acs.org/jmc

Halogenated 2′-Benzoylpyridine Thiosemicarbazone (XBpT) Chelators with Potent and Selective Anti-Neoplastic Activity: Relationship to Intracellular Redox Activity

Christian Stefani,[†] Gaya Punnia-Moorthy,[†] David B. Lovejoy,[†] Patric J. Jansson,[†] Danuta S. Kalinowski,[†] Philip C. Sharpe,[‡] Paul V. Bernhardt,[‡] and Des R. Richardson*[,†]

[†]Iron Metabolism and Chelation Program, Department of Pathology, University of Sydney, Sydney, NSW, 2006, Australia

[‡]Centre for Metals in Biology, School of Chemistry and Molecular Biosciences, University of Queensland, Brisbane, Qld 4072 Australia

Supporting Information

ABSTRACT: Iron chelators of the 2′-benzoylpyridine thiosemicarbazone (BpT) class show substantial potential as anticancer agents. To explore structure−activity relationships, new BpT analogues were designed that incorporated halogen substituents on the noncoordinating phenyl group (XBpTs). These XBpT ligands exhibited potent antiproliferative activity with some analogues exceeding that of the parent BpT compound. Importantly, there was an appreciable therapeutic index in vitro, as mortal cells were significantly less affected by these chelators relative to neoplastic cells. The addition of a halogen led to a halogen-specific increase in the redox potential of XBpT−Fe complexes. Probing for chelator-induced intracellular reactive oxygen species (ROS) with the fluorescent probe, 2′,7′-dichlorofluorescein, revealed a 1.5−4.7-fold increase in fluorescence upon incorporation of Cl, Br, or I to the parent analogues. Furthermore, an important structure−activity relationship was deduced where the addition of halogens led to a positive correlation between intracellular ROS generation and antiproliferative activity in the more hydrophilic BpT parent compounds.

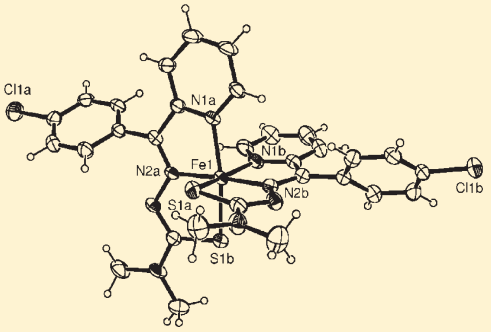

INTRODUCTION

The traditional use of iron (Fe) chelators is for the treatment of Fe overload diseases.[1−4] However, their use in cancer therapy has emerged as a potentially fruitful area of investigation.[5−7] Iron is essential for proliferation, and the increased requirement for Fe in rapidly dividing cells leads to an enhanced sensitivity of tumor cells to Fe-deprivation as compared to normal cells. This increased requirement for Fe is reflected in cancer cells relative to their normal counterparts by the increased expression of the transferrin receptor 1, which is involved in Fe uptake from transferrin (Tf).[8]

Iron chelators can sequester Fe from biological systems and, hence, are able to inhibit the activity of Fe-requiring proteins, including ribonucleotide reductase, a key enzyme that is involved in the rate-limiting step of DNA synthesis.[9−11] However, the potent antiproliferative activity of some Fe chelators is likely mediated by their effects on multiple molecular targets.[12−15] Chelators with potent antiproliferative activity, such as the thiosemicarbazones, also demonstrate the ability to form Fe complexes capable of redox cycling.[16−20] This leads to the generation of reactive oxygen species (ROS) such as hydroxyl radicals, which induce cellular injury including DNA damage.[16−20]

Previous studies using the Fe chelator, desferrioxamine (DFO; Figure 1A), showed that it induced modest antitumor efficacy in vitro and in vivo.[5,15,16] The poor membrane permeability of DFO limits its activity and application in cancer therapy.[21−24] However, these findings have led to research examining novel Fe chelators as cancer chemotherapeutics.[25,26] More hydrophobic Fe chelators, such as 3-aminopyridine-2-carboxaldehyde thiosemicarbazone (3-AP; Figure 1A), have since been investigated as potential anticancer therapeutics. In fact, 3-AP has been investigated in several phase I and phase II clinical trials.[27−29]

Chelators previously developed within our laboratory, namely, the di-2′-pyridylketone thiosemicarbazone (DpT) series, exhibited potent and selective antiproliferative activity.[18] In particular, di-2-pyridylketone 4,4-dimethyl-3-thiosemicarbazone (Dp44mT; Figure 1A) demonstrated the highest activity of all ligands within this series.[18] Dp44mT showed marked and selective activity in vivo, reducing the growth of a murine M109 lung cancer by approximately 50% after 5 days of treatment, while having little effect on hematological indices.[18] In addition, initial studies indicated that the Fe complex was redox-active within cells.[18] More recently, Dp44mT has shown marked and selective activity in vivo against a panel of human tumor xenografts in nude mice.[30] However, at high nonoptimal doses, this agent leads to cardiac fibrosis and weight loss.[30] The electrochemistry of the Fe complexes of the DpT analogues showed facile interconversion between the Fe^{II} and the Fe^{III} states within the range accessible to cellular oxidants and

Received: July 13, 2011
Published: August 16, 2011

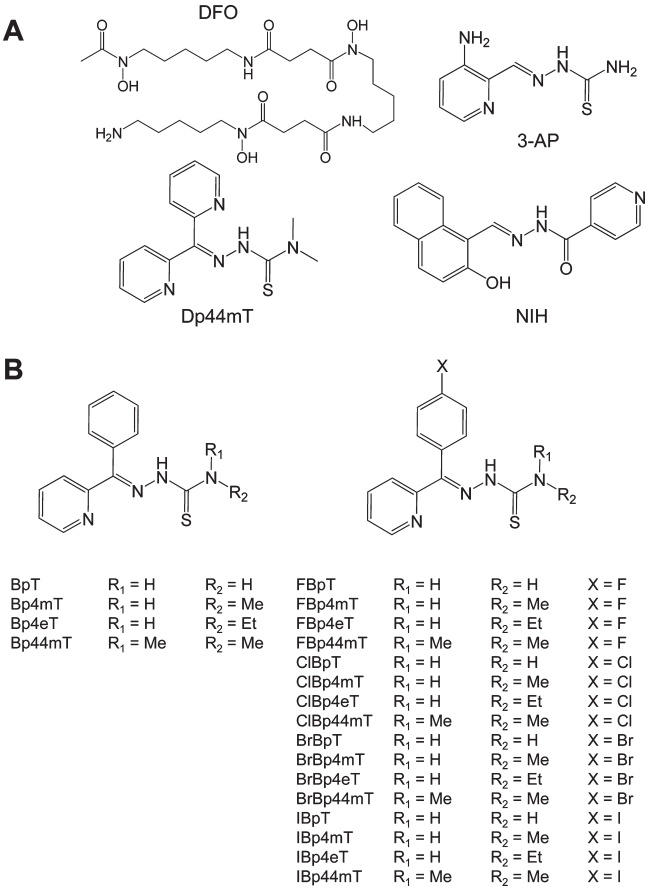

BpT	R_1 = H	R_2 = H	FBpT	R_1 = H	R_2 = H	X = F
Bp4mT	R_1 = H	R_2 = Me	FBp4mT	R_1 = H	R_2 = Me	X = F
Bp4eT	R_1 = H	R_2 = Et	FBp4eT	R_1 = H	R_2 = Et	X = F
Bp44mT	R_1 = Me	R_2 = Me	FBp44mT	R_1 = Me	R_2 = Me	X = F
			ClBpT	R_1 = H	R_2 = H	X = Cl
			ClBp4mT	R_1 = H	R_2 = Me	X = Cl
			ClBp4eT	R_1 = H	R_2 = Et	X = Cl
			ClBp44mT	R_1 = Me	R_2 = Me	X = Cl
			BrBpT	R_1 = H	R_2 = H	X = Br
			BrBp4mT	R_1 = H	R_2 = Me	X = Br
			BrBp4eT	R_1 = H	R_2 = Et	X = Br
			BrBp44mT	R_1 = Me	R_2 = Me	X = Br
			IBpT	R_1 = H	R_2 = H	X = I
			IBp4mT	R_1 = H	R_2 = Me	X = I
			IBp4eT	R_1 = H	R_2 = Et	X = I
			IBp44mT	R_1 = Me	R_2 = Me	X = I

Figure 1. (A) Chemical structures of the iron chelators: 3-AP, DFO, 2-hydroxy-1-naphthaldehyde isonicotinoyl hydrazone (NIH), and di-2-pyridylketone 4,4-dimethyl-3-thiosemicarbazone (Dp44mT). (B) Chemical structures of members of the 2′-benzoylpyridine thiosemicarbazone (BpT) series of ligands and their halogenated counterparts. The current studies investigated the impact of incorporating halogen atoms (F, Cl, Br, or I) on the phenyl ring of the BpT series ligands to generate XBpT analogues, 2′-benzoylpyridine 4-methyl-3-thiosemicarbazone (Bp4mT) analogues, 2′-benzoylpyridine 4-ethyl-3-thiosemicarbazone (Bp4eT) analogues, and 2′-benzoylpyridine-4,4-dimethyl-3-thiosemicarbazone (Bp44mT) analogues.

reductants (~+100 to +250 mV vs NHE),[31] making them ideal catalysts of Fenton chemistry. This suggests that the antitumor activity of these chelators is due, at least in part, to both their ability to bind intracellular Fe and form redox-active complexes, inducing oxidative damage.[31,32]

Substitution of the noncoordinating 2-pyridyl moiety on the DpT series with a phenyl ring generated the 2′-benzoylpyridine thiosemicarbazone (BpT; Figure 1B) series. The BpT series exhibited enhanced antiproliferative efficacy relative to their DpT homologues.[33] In particular, 2′-benzoylpyridine 4-ethyl-3-thiosemicarbazone (Bp4eT; Figure 1B) demonstrated the highest activity of all ligands within this series in vitro (IC_{50}, 0.002 μM).[33] Recent studies in vivo using nude mice bearing a human DMS-53 lung cancer xenograft showed that the BpT series analogue, 2′-benzoylpyridine-4,4-dimethyl-3-thiosemicarbazone (Bp44mT), can be administered intravenously or orally with potent antitumor efficacy.[34] Importantly, in contrast to Dp44mT, Bp44mT has the marked advantage of not causing cardiac toxicity or weight loss, even when administered at much higher doses.[34]

Electrochemistry of the Fe complexes of the BpT analogues revealed lower $Fe^{III/II}$ redox potentials (+99 to +180 mV vs NHE) than their DpT homologues.[33] The lower electron-withdrawing property of the phenyl moiety in the BpT series relative to the pyridyl ring in the DpT series probably contributes toward the lowered $Fe^{III/II}$ redox potentials of the BpT−Fe complexes.[33] This factor leads to their higher redox activity, as shown by ascorbate oxidation and benzoate hydroxylation studies, which demonstrated that the Fe^{III}−BpT complexes were able to redox cycle and stimulate redox reactions to a greater degree than the corresponding Fe^{III}−DpT complexes.[33]

Considering the marked activity of the BpT analogues[33] and to gain further insight into chelator structure−activity relationships, we investigated the impact of incorporating halogens on the phenyl ring to generate 2-(4′-halobenzoyl)pyridine thiosemicarbazone (XBpT; Figure 1B) analogues. In particular, we have chosen four BpT analogues of increasing lipophilicity, namely: BpT, 2′-benzoylpyridine 4-methyl-3-thiosemicarbazone (Bp4mT), Bp4eT, and Bp44mT, each of which were halogenated on the noncoordinating phenyl ring with either F, Cl, Br, or I (Figure 1B). Halogenation is expected to both enhance the lipophilicity of the molecule and also to subtly alter the electrochemistry of the chelator−iron complex. The major findings from these studies are the link between antiproliferative efficacy and redox activity and the structure−activity relationships that pertain to this, namely: (i) the correlation between lipophilicity and intracellular redox stress and (ii) establishment of the concept of a threshold for redox activity and its relationship to antiproliferative efficacy. In addition, the potencies of the new halogenated compounds are in general superior to the parent analogues with an appreciable therapeutic index being observed.

RESULTS AND DISCUSSION

Synthesis and Spectroscopy. The XBpT analogues were all prepared by high-yielding Schiff base condensation reactions following previous protocols for related thiosemicarbazones reported from our laboratory.[31,33] The compounds were only sparingly soluble in water. However, they exhibited greater solubility in polar aprotic solvents such as DMF, MeCN, and DMSO. The ^{1}H NMR spectral properties of the XBpT ligands are very similar to those of the BpT analogues.[33]

Structural Characterization. As representative members of the XBpT series, the crystal structures of FBp44mT, ClBp44mT, BrBp44mT, and IBp44mT have been determined (Figure 1S A−D in the Supporting Information). Crystal data are in Table 1S (Supporting Information), and selected bond lengths and angles are included in Table 2S (Supporting Information). The most obvious variations are to the C−X (X = F, Cl, Br, or I) bond length due to the increasing covalent radius of the halogen. An unexpected, but significant, variation across the series is found in the N3−C13 bond, which increases (from the F through to the I analogue; Table 2S in the Supporting Information). Interestingly, this was not correlated with any other variations in bond lengths. The C13−S1 bonds are consistent with double bonds,[31] while the N3−C13 bond is typical of a thioamide (intermediate bond order). In each structure, intramolecular H-bonding (N3−H···N1) is a feature that fixes the conformation of the ligand in a way that is unsuitable for coordination through the N1, N2, and S1 set of donors. This is discussed below when

dx.doi.org/10.1021/jm200924c |J. Med. Chem. 2011, 54, 6936–6948

Table 1. Partition Coefficients (Log P_{calcd}) and $Fe^{III/II}$ Redox Potentials (MeCN:H_2O 7:3) of the XBpT Series Chelators and Their Ferrous and Ferric Complexes[a]

ligand	partition coefficient (log P_{calcd})	$Fe^{II/III}$ redox potential (mV vs NHE)
NIH	2.63	
Dp44mT	2.19	113
BpT	2.25	104
FBpT	2.41	131
ClBpT	2.81	137
BrBpT	3.08	142
IBpT	3.6	138
Bp4mT	2.77	79
FBp4mT	2.93	93
ClBp4mT	3.33	103
BrBp4mT	3.6	101
IBp4mT	4.13	104
Bp4eT	3.11	66
FBp4eT	3.26	91
ClBp4eT	3.66	95
BrBp4eT	3.93	94
IBp4eT	4.46	102
Bp44mT	3.14	63
FBp44mT	3.3	82
ClBp44mT	3.7	99
BrBp44mT	3.97	107
IBp44mT	4.5	98

[a] Comparable data for the parent BpT compounds, Dp44mT and NIH, are also shown. Log P_{calcd} values were calculated using the program ChemBioDraw Ultra v 11.0.1 using Crippen's fragmentation procedure.[42]

considering the structures of the Fe complexes and their biological activity as antitumor agents.

Fe Coordination Chemistry. The Fe^{III} complexes of each series were isolated and characterized. Their electronic spectral properties mirror those of the respective $[Fe^{III}(BpT)_2]^+$ analogues.[33] As relative examples, the crystal structures of $[Fe^{III}(ClBp44mT)_2]ClO_4$ and of $[Fe^{III}(FBp44mT)_2](ClO_4)\cdot$MeCN were determined, and the complex cations are shown in Figure 1SE,F (Supporting Information). The coordination spheres of the Fe centers are very similar, and the bond lengths are consistent with low spin Fe^{III} complexes.[35] There are major differences in the bond lengths within the N3−C13−S1 group brought about by deprotonation of N3 and coordination of S1 in both complexes (Table 2S in the Supporting Information). It is apparent that C13−S1 takes on single bond character, while C13−N3 shortens by comparison with the structures of the neutral free ligands (Table 2S in the Supporting Information). The anionic ligands are coordinated in a tridentate manner dominantly in their imine-thiolate resonance form. The dimethylamino groups of the ligands are coplanar with the −C(S)NN group in these structures and in those of the free ligands. Note that the conformations of the coordinated ligands (with the three donor atoms in a *syn* disposition) are distinctly different to those of the free ligands. These data demonstrating Fe complexation are significant, as the antitumor efficacy of this general class of ligands is due to two major properties, namely, their cellular Fe-binding efficacy and ability to form cytotoxic, redox-active Fe complexes.[33]

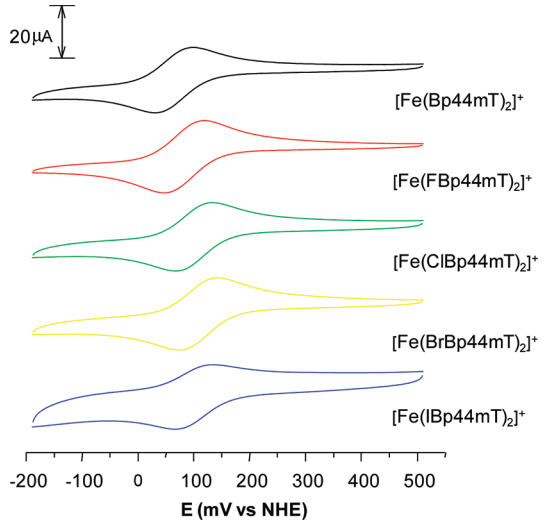

Figure 2. Cyclic voltammograms of 1 mM solutions of $[Fe(Bp44mT)_2]^+$, $[Fe(FBp44mT)_2]^+$, $[Fe(BrBp44mT)_2]^+$, and $[Fe(IBp44mT)_2]^+$ (from top to bottom) showing the impact of incorporation of a halogen atom on the $Fe^{III/II}$ redox potential. Sweep rate, 100 mV s^{-1}; solvent MeCN:H_2O (70:30) with 0.1 M Et_4NClO_4.

Electrochemistry. The electrochemical properties of the Fe complexes of the XBpT analogues constituted a crucial part of this study due to the relevance of this property to their biological activity.[33] Indeed, the antiproliferative activity of related ligands reported by us previously is likely linked with their capability to undergo Fenton chemistry upon complexation with intracellular Fe.[20,31,33,35,36] All compounds exhibited totally reversible one electron $Fe^{III/II}$ couples in MeCN:H_2O (7:3) at sweep rates between 50 and 500 mV s^{-1}. This solvent combination was chosen to ensure that (i) sufficient solubility, as these compounds are largely insoluble in water, and (ii) to enable comparisons with similar compounds (i.e., BpT analogues) reported in our previous studies where the same solvent was used.[33] Other solvent combinations such as DMF:H_2O (4:1) also gave similar electrochemistry. The redox potentials of the Fe complexes are collected in Table 1 and may be compared with those of the $[Fe(BpT)_2]^+$ complexes.[33]

The anodic shift in the $Fe^{II/III}$ redox potentials of the XBpT complexes in comparison to their corresponding BpT−Fe complexes is apparent from Figure 2 and Table 1. As an example, the cyclic voltammograms of four Fe^{III} complexes, namely, $[Fe(FBp44mT)_2]^+$, $[Fe(ClBp44mT)_2]^+$, $[Fe(BrBp44mT)_2]^+$, and $[Fe(IBp44mT)_2]^+$ bearing the same terminal substituent ($-NMe_2$) are shown in Figure 2. Generally, the redox potentials of the halo-substituted complexes were anodically shifted by 14−44 mV relative to their BpT counterparts, as would be expected from the electron-withdrawing, inductive effects of these substituents. However, smaller than expected shifts of 7−16 mV were observed within the four halo-substituted complexes of each set (e.g., $[Fe(XBpT)_2]^{+/0}$ X = F, Cl, Br, or I). The only exception to this latter effect was $[Fe(BrBp44mT)_2]^{+/0}$, with an anodic shift of 25 mV relative to its F- analogue.

The effect of the identity of the N4 substituent on the $Fe^{III/II}$ redox potential was similar within the four halo-substituted complexes of each set (e.g., $[Fe(XBpT)_2]^{+/0}$ X = F, Cl, Br, or I). That is, methylation, ethylation, or dimethylation at N4 led to a cathodic shift of 34−49 mV relative to the $[Fe(XBpT)]^+$ parent complex.

Table 2. IC_{50} (μM) Values of XBpT Series Chelators at Inhibiting the Growth of SK-N-MC Neuroepithelioma Cells and Mortal MRC-5 Lung Fibroblasts as Determined by the MTT Assay[a]

	IC_{50} (μM)			
ligand	SK-N-MC	MRC-5	p value	therapeutic index
DFO	22.7 ± 1.55			
NIH	2.53 ± 0.18			
Dp44mT	0.004 ± 0.001			
BpT	5.589 ± 0.299	>25	$p < 0.001$	
FBpT	2.534 ± 0.169	>25	$p < 0.001$	
ClBpT	0.356 ± 0.026	16.66 ± 0.407	$p < 0.001$	47
BrBpT	0.321 ± 0.072	8.198 ± 1.498	$p < 0.005$	26
IBpT	0.172 ± 0.046	6.980 ± 1.662	$p < 0.005$	41
Bp4mT	0.024 ± 0.000	2.321 ± 0.208	$p < 0.001$	96
FBp4mT	0.022 ± 0.001	2.468 ± 0.008	$p < 0.001$	112
ClBp4mT	0.013 ± 0.002	1.967 ± 0.155	$p < 0.001$	148
BrBp4mT	0.011 ± 0.002	1.011 ± 0.167	$p < 0.001$	93
IBp4mT	0.010 ± 0.001	0.959 ± 0.084	$p < 0.001$	98
Bp4eT	0.012 ± 0.001	0.738 ± 0.100	$p < 0.001$	64
FBp4eT	0.010 ± 0.001	0.732 ± 0.108	$p < 0.001$	71
ClBp4eT	0.009 ± 0.001	0.586 ± 0.062	$p < 0.001$	65
BrBp4eT	0.009 ± 0.002	0.498 ± 0.038	$p < 0.001$	53
IBp4eT	0.010 ± 0.001	0.461 ± 0.023	$p < 0.001$	46
Bp44mT	0.009 ± 0.001	1.012 ± 0.106	$p < 0.001$	116
FBp44mT	0.008 ± 0.001	0.794 ± 0.171	$p < 0.001$	102
ClBp44mT	0.007 ± 0.001	0.706 ± 0.008	$p < 0.001$	96
BrBp44mT	0.008 ± 0.001	0.571 ± 0.093	$p < 0.001$	72
IBp44mT	0.009 ± 0.002	0.633 ± 0.004	$p < 0.001$	68

[a] Cells were seeded and allowed to attach to wells for 24 h/37 °C and then incubated for 72 h/37 °C with control medium or the chelators. Results are means ± SDs (three experiments). The p values were determined using Student's t test and compared the activity of the ligand using normal and neoplastic cells. Therapeutic index values represent the ratio of MRC-5 to SK-N-MC IC_{50} values; a higher therapeutic index value indicates greater selectivity for neoplastic cells.

Overall, the anodic shift in potential resulting from incorporation of a halogen to the noncoordinating phenyl group is offset by the cathodic shift resulting from alkylation at N4. In relation to biological activity, all measured $Fe^{II/III}$ redox potentials lie within the range accessible to both cellular oxidants and reductants, and both the ferric and the ferrous forms are chemically stable. Hence, like their BpT counterparts,[33] these halogen-substituted compounds could redox cycle to generate intracellular ROS (examined below).

BIOLOGICAL STUDIES

Antiproliferative Activity against Tumor Cells. The ability of the XBpT series to inhibit cellular proliferation was assessed using SK-N-MC neuroepithelioma cells, as the effect of Fe chelators on their growth has been well characterized.[31,33,37] These novel ligands were compared to their parent compounds, the BpT series,[33] and a number of relevant positive control chelators. These included DFO, which is used for the treatment of Fe overload; 2-hydroxy-1-naphthylaldehyde isonicotinoyl hydrazone (NIH), a ligand with high iron mobilizing activity and moderate antiproliferative activity;[37] and Dp44mT, a chelator with high antiproliferative activity extensively studied for cancer therapy[16,18] (Figure 1A). These results are presented in Table 2. This study identified all of the N4 substituted XBpT analogues [i.e., 2′-(4″-halobenzoyl)pyridine 4-methyl-3-thiosemicarbazone (XBp4mT), 2′-(4″-halobenzoyl)pyridine 4-ethyl-3-thiosemicarbazone (XBp4eT), and 2′-(4″-halobenzoyl)pyridine 4,4-dimethyl-3-thiosemicarbazone (XBp44mT)] as having high antiproliferative activity (IC_{50}, 0.007−0.024 μM), which was similar to that observed for Dp44mT (IC_{50}, 0.004 μM), but significantly ($p < 0.001$) more effective than either DFO or NIH. All of the XBpT ligands examined were significantly ($p < 0.01$) more active than DFO (IC_{50}, 22.7 μM), and excluding FBpT, these halogenated ligands were significantly ($p < 0.01$) more active than NIH (IC_{50}, 2.53 μM). Our previous studies examining the DpT ligands against a wide range of neoplastic cell types in vitro indicated that these agents show broad and marked antiproliferative activity against 28 different neoplastic cell types.[30] Additionally, our DpT and BpT chelators demonstrate antitumor activity against a range of human tumor xenografts in vivo in nude mice.[18,30,34] Hence, we would expect that the very closely related XBpT series to show similar broad anticancer activity.

The addition of halogens of increasing atomic weight to the parent BpT ligand led to the most marked and significant ($p < 0.001$) increase in antiproliferative activity against SK-N-MC neuroepithelioma cells, where the IC_{50} decreased 32-fold from 5.59 (BpT) to 0.17 μM (IBpT; Table 2). This marked enhancement in efficacy is believed to be due to the effect of the halogens on the overall lipophilicity of the ligand (Table 1). The addition of Cl, Br, or I to the Bp4mT ligand led to a more modest but significant ($p < 0.01$) increase in antiproliferative activity, where the IC_{50} decreased 2.4-fold from 0.024 (Bp4mT) to 0.010 μM (IBp4mT; Table 2). In contrast, halogenation of the more lipophilic Bp4eT (IC_{50}, 0.012 μM) and Bp44mT (IC_{50}, 0.009 μM) produced ligands of comparable antiproliferative efficacy. These observations suggested an important structure−activity relationship. That is, for the BpT and Bp4mT series ligands, addition of halogens to the noncoordinating phenyl group generated analogues with lipophilicities optimal for membrane permeability and antiproliferative activity. However, for the Bp4eT and Bp44mT series of chelators, an optimal lipophilicity appeared to have already been achieved. Hence, the addition of a halogen had little effect on antiproliferative efficacy, which was already marked for the parent ligands (i.e., Bp4eT and Bp44mT).

Plotting the octanol:water partition coefficients ($\log P_{calcd}$) for the chelators against their antiproliferative activity (IC_{50}) in SK-N-MC cells demonstrated that an optimal lipophilic range existed, with the ligands possessing the highest antiproliferative activity having $\log P_{calcd}$ values between 3.1 and 4.5, with optimal efficacy being observed at a $\log P_{calcd}$ of ~4 (Figure 3A). It should be noted that for this analysis the XBpT analogues and the respective parent compound (BpT) were excluded due to their low activity. Considering this, it is likely that compounds of this class with $\log P_{calcd}$ values outside 3.1−4.5 will either have difficulty traversing the cell membrane or become trapped within membranes due to their high affinity for the lipid environment. Previous studies have also indicated the importance of the relationship between optimal lipophilicity and antiproliferative activity.[16,37] In fact, a similar parabolic relationship between the lipophilicity and the efficacy of iron chelation has been observed examining a series of tridentate aroylhydrazone ligands.[38]

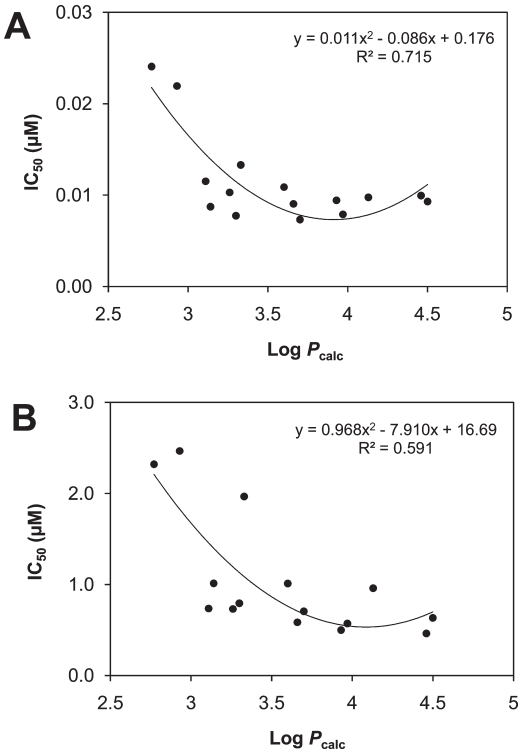

Figure 3. Relationship between the antiproliferative activity and lipophilicity of the chelators using: (A) SK-N-MC neuroepithelioma cells or (B) MRC-5 lung fibroblasts. The IC_{50} and log P_{calcd} values for the XBp4mT, XBp44mT, and XBp4eT analogues and their parent compounds (Bp4mT, Bp44mT, and Bp4eT) were plotted. However, the XBpT analogues and the respective parent compound (BpT) were excluded due to their high IC_{50} values.

Antiproliferative Activity against Normal Cells. For a compound to be considered as an antitumor agent, it must exhibit potent antiproliferative activity against neoplastic cells, while leaving normal cells unaffected. To determine whether the compounds exhibited selectivity toward neoplastic cells, the effect on the proliferation of mortal MRC-5 fibroblasts was assessed (Table 2). Comparison of the antiproliferative activity of the chelators between SK-N-MC neuroepithelioma cells and MRC-5 fibroblasts showed that the neoplastic cells were significantly ($p < 0.005-0.001$) more sensitive than the normal cells, suggesting an appreciable therapeutic index. In contrast to the results found for the SK-N-MC tumor cells, where only halogenation of the BpT and Bp4mT analogues led to increased antiproliferative activity, it was of interest that using mortal MRC-5 cells, halogenation increased activity in all series. However, it was notable that as found for SK-N-MC cells, the increase in antiproliferative efficacy upon halogenation was most pronounced for the BpT series (Table 2).

The in vitro therapeutic index was also calculated. This parameter represents the ratio of the IC_{50} values of MRC-5 to SK-N-MC cells (i.e., IC_{50} MRC-5/IC_{50} SK-N-MC; Table 2), with higher values representing greater selectivity against tumor cells. The XBp4mT series showed the greatest selectivity, with ClBp4mT being the most selective ligand examined. Plotting the octanol:water log P_{calcd} for the chelators against IC_{50} found in mortal MRC-5 cells revealed that as found for neoplastic SK-N-MC cells (Figure 3A), a very similar optimal lipophilic range exists, with all ligands possessing the highest antiproliferative activity having log P_{calcd} values between 3.1 and 4.5 (Figure 3B). Again, the XBpT analogues and the BpT parent ligand were excluded to enable a comparison to neoplastic cells (Figure 3A).

Chelator-Mediated ^{59}Fe Efflux from Cells. To determine the potential role of Fe chelation efficacy in the antiproliferative activity of the XBpT analogues, the ability of these chelators to mobilize intracellular ^{59}Fe from prelabeled SK-N-MC neuroepithelioma cells was examined (Figure 4A). The release of ^{59}Fe mediated by these ligands was compared to that of their parent BpT compounds, as well as a number of positive controls, including the chelators DFO, NIH, and Dp44mT (Figure 1A), which have been characterized in detail in this cell type.[9,18,37]

Both of the positive controls, NIH and Dp44mT, showed high ^{59}Fe mobilization activity, releasing 55 ± 1 and 53 ± 1% of intracellular ^{59}Fe, respectively (Figure 4A). In comparison, the control that was culture media alone mediated 10 ± 1% of intracellular ^{59}Fe release. As shown previously,[18,33] the clinically used chelator, DFO, demonstrated limited ^{59}Fe mobilization efficacy, resulting in the release of only 23 ± 1% of intracellular ^{59}Fe (Figure 4A). All 16 members of the XBpT analogues demonstrated significant ^{59}Fe mobilization activity, resulting in the release of 34−56% of cellular ^{59}Fe. The XBp4mT series of ligands, FBp4mT, ClBp4mT, and BrBp4mT, demonstrated the greatest ^{59}Fe chelation efficacy (51−56% of cellular ^{59}Fe released; Figure 4A), having comparable ^{59}Fe mobilization activity to NIH and Dp44mT. The XBp4eT and XBp44mT ligands showed very similar activity that was slightly less than their homologous Bp4mT counterparts, leading to the release of 34−48% of cellular ^{59}Fe.

Within each series, incorporation of a halogen moiety led to a molecular weight-dependent decline in ^{59}Fe mobilization activity, the starkest of which was observed for the XBp4eT and XBp44mT series. Within all four groups of BpT analogues, the addition of I to the noncoordinating phenyl group of the parent compound resulted in a significant ($p < 0.001$) decrease of Fe chelation efficacy (Figure 4A). In fact, the iodinated chelator represents the most lipophilic halogenated ligand in each group (Table 1), and as such, may become entrapped within membranes through their high affinity for the lipid environment, reducing ^{59}Fe efflux. It should be noted that the chelator-mediated increase in cellular ^{59}Fe mobilization was not mediated by their cytotoxic effects, as the cells remained >99% viable (as judged by Trypan blue staining) within the very short 3 h incubation used in these assays.

Chelator-Mediated Inhibition of Cellular ^{59}Fe Uptake from ^{59}Fe-Tf. The ability of the XBpT series chelators to inhibit ^{59}Fe uptake from the Fe-binding protein, Tf, by SK-N-MC neuroepithelioma cells was also assessed (Figure 4B). This is important, as inducing Fe deprivation and thus antiproliferative activity involves both increasing Fe mobilization and preventing Fe uptake from Tf.[37] As demonstrated in our previous work,[9,18] the positive controls, NIH and Dp44mT, were found to effectively reduce ^{59}Fe uptake to 6 ± 1 and 4 ± 1% of the control, respectively (Figure 4B). In contrast, the hydrophilic chelator, DFO, exhibited far less activity, as shown previously,[37−39] reducing ^{59}Fe uptake to only 74 ± 1% of the control (Figure 4B).

All members of the XBpT series markedly reduced ^{59}Fe uptake to between 4 and 32% of the control (Figure 4B), being significantly ($p < 0.01$) more effective than DFO. All of the ligands examined, except BpT, FBpT, and ClBpT, were significantly ($p < 0.05$) less effective than both Dp44mT and NIH at inhibiting ^{59}Fe uptake from ^{59}Fe-Tf. The XBpT series of ligands

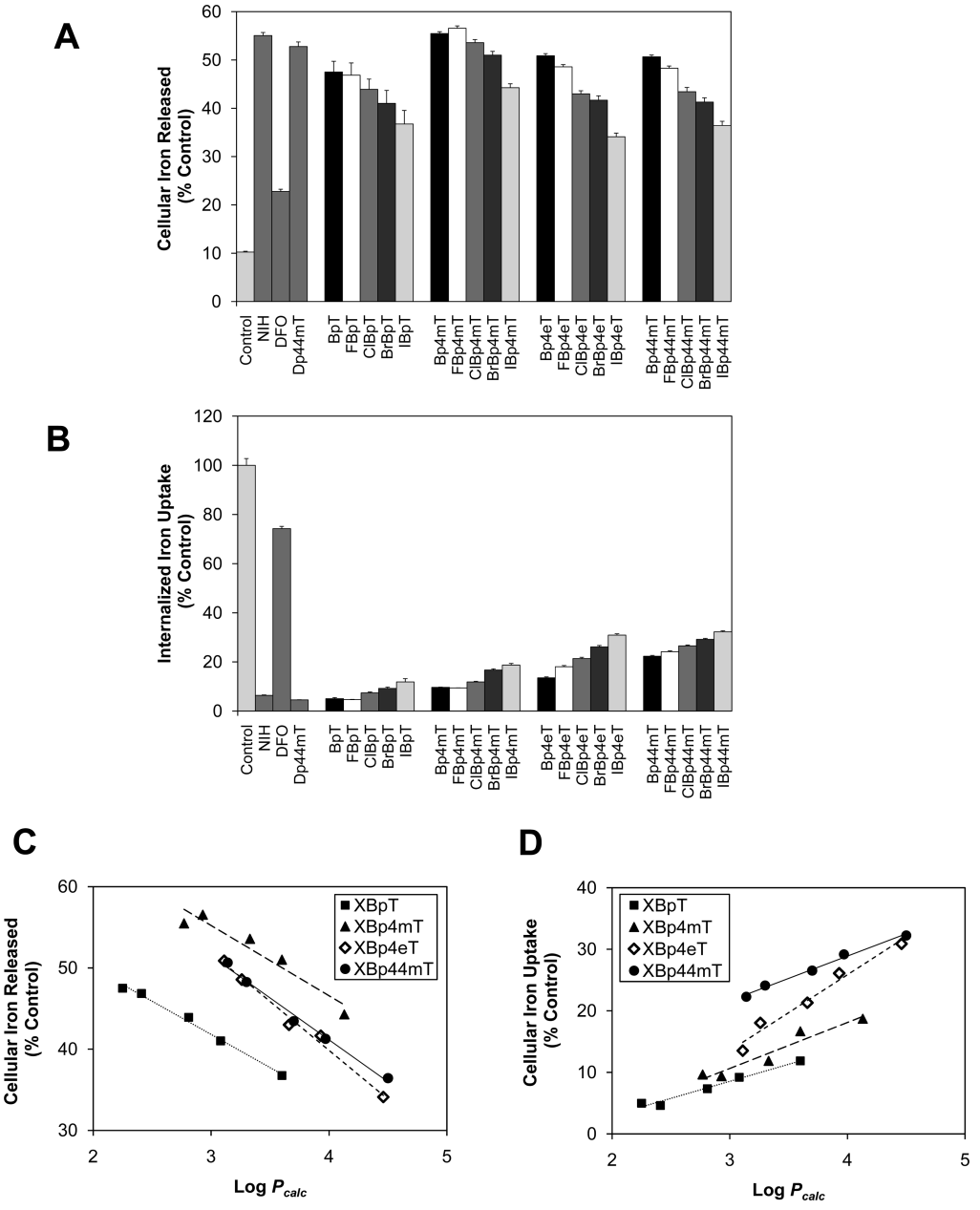

Figure 4. Effect of the XBpT series chelators on (A) ^{59}Fe mobilization from prelabeled SK-N-MC neuroepithelioma cells and (B) ^{59}Fe uptake from ^{59}Fe-Tf by SK-N-MC neuroepithelioma cells. Results are means ± SDs of three experiments with three determinations in each experiment. The relationship between (C) ^{59}Fe uptake and lipophilicity (log P_{calcd}) and (D) ^{59}Fe mobilization and lipophilicity (log P_{calcd}) for each examined ligand.

were the most effective at reducing ^{59}Fe uptake from ^{59}Fe-Tf, decreasing it to 4−12% of the control (Figure 4B). As observed in the ^{59}Fe efflux experiments (Figure 4A), incorporation of a halogen again led to a molecular weight-dependent reduction in activity, with the I-containing analogue having the least activity at preventing ^{59}Fe uptake in each case. This relationship can be seen most clearly when ^{59}Fe efflux and uptake results are plotted against the lipophilicity (log P_{calcd}) of the chelators (Figure 4C,D). Within each series, a linear relationship was observed between ^{59}Fe efflux or ^{59}Fe uptake relative to lipophilicity, demonstrating the important role of optimum lipophilicity in their ability to bind cellular iron pools that are crucial for proliferation.[5,16,26]

Ascorbate Oxidation Studies. The electrochemical studies reported in Table 1 demonstrated the facile interconversion between the Fe^{III} and Fe^{II} states at potentials accessible to biological oxidants and reductants. To determine if redox activity played a role in the compounds' antiproliferative activity, their ability to catalyze the oxidation of a physiologically relevant substrate, ascorbate, was evaluated. The in vitro oxidation of ascorbate by Fe complexes of the XBpT series was examined, in both comparison to their parent BpT analogues and the positive control, EDTA (Figure 5). EDTA was included as its activity has been well characterized in this assay.[33,35,40]

In all experiments, results were expressed as iron-binding equivalents (IBEs). This was due to the different coordination modes of the ligands to Fe, that is, EDTA is hexadentate and

dx.doi.org/10.1021/jm200924c |J. Med. Chem. 2011, 54, 6936–6948

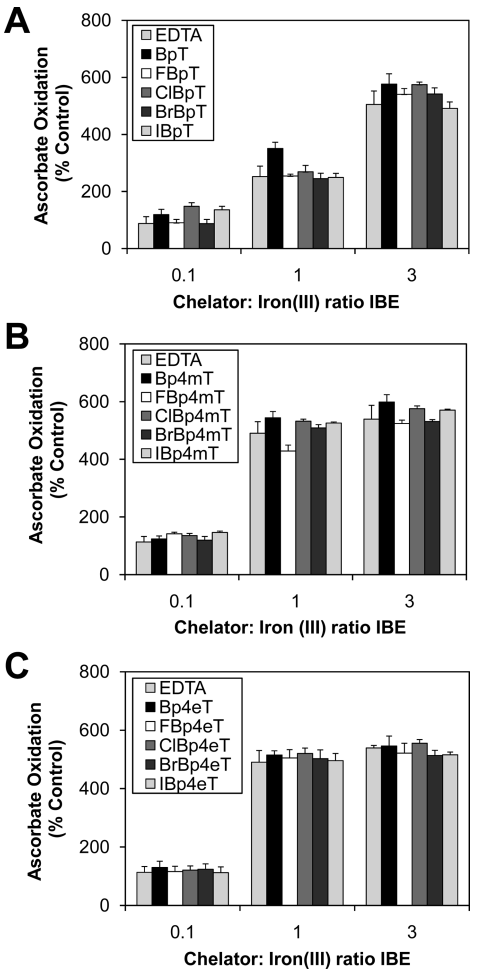

Figure 5. Effect of the Fe^{III} complexes of the (A) XBpT, (B) XBp4mT, and (C) XBp4eT series and their parent compounds on ascorbate oxidation. Chelators at iron-binding equivalent (IBE) ratios of 0.1, 1, and 3 were incubated in the presence of Fe^{III} (10 μM) and ascorbate (100 μM). The UV−vis absorbance at 265 nm was recorded after 10 and 40 min, and the difference between the time points was calculated. Comparison of these chelators is made to the positive control, EDTA. The XBp44mT series of compounds could not be measured due to precipitation of the ligand using these assay conditions. Results are means ± SDs (three experiments).

forms 1:1 ligand:Fe complexes, while the BpT and XBpT analogues are tridentate (Figure 1S in the Supporting Information),[33] resulting in 2:1 ligand:Fe complexes. In the present study, a range of ligand:Fe IBE ratios were used, namely, 0.1, 1, or 3. An IBE of 0.1 represents an excess of Fe, where one hexadentate or two tridentate ligands are in the presence of 10 Fe atoms. An IBE of 1 results in complete filling of the coordination sphere, while an IBE of 3 represents an excess of the ligand, where three hexadentate or six tridentate ligands are in the presence of one Fe atom.[31]

In good agreement with our previous studies, EDTA markedly increased ascorbate oxidation at an IBE of 1 and 3, respectively, while showing little activity at an IBE of 0.1 (Figure 5A−C). This is in agreement with previous studies demonstrating the ability of the EDTA−Fe complex to undergo facile redox cycling and catalyze ascorbate oxidation.[33,35,40] Generally, halogenation did not markedly affect the ability of the BpT, Bp4mT, or Bp4eT analogues to catalyze Fe^{III}-mediated ascorbate oxidation at IBE ratios of 0.1, 1, or 3, with all compounds being similar to EDTA in each case (Figure 5A−C). The ascorbate oxidation activity of the XBp44mT series could not be measured with certainty, as under the reaction conditions used, the compounds precipitated from solution. Hence, these results are not shown.

Collectively, these ascorbate oxidation results indicate that the incorporation of a halogen to the noncoordinating phenyl group of the BpT series does not appreciably affect their ability to mediate ascorbate oxidation; hence, their redox activity remained marked. These results are also in agreement with the electrochemical data presented, which demonstrated that the Fe complexes of the XBpT series exhibited comparable redox potentials to their parent BpT counterparts (Table 1), enabling ascorbate oxidation.

Intracellular ROS Assay. To confirm the redox activity of the XBpT analogues as suggested by the electrochemical and ascorbate oxidation studies, further studies assessed their potential to generate ROS intracellularly. The degree of cellular ROS was examined by probing for oxidation of the nonfluorescent molecule, 2′,7′-dichlorodihydrofluorescein (H_2DCF), which becomes fluorescent when oxidized to 2′,7′-dichlorofluorescein (DCF). The use of this probe represents an established protocol for assessing intracellular redox stress.[18,41] Hydrogen peroxide (H_2O_2) was included as a positive control.[18]

Incubation of cells with all analogues studied (except BpT) led to a shift of the DCF fluorescence peak to the right relative to control cells. Indeed, as appropriate examples in Figure 6A, we present flow cytometry profiles of the parent compound of each series (BpT, Bp4mT, Bp4eT, and Bp44mT) and their respective I-substituted analogues. This shift is marked for the halogenated analogues (shaded in gray) relative to the parent compounds and reflects an increase in the intracellular oxidation of H_2DCF to fluorescent DCF. The DCF fluorescence peaks for each compound evaluated were quantified and are shown in Figure 6B. These data reveal a significant ($p < 0.01$) increase in DCF fluorescence for the parent compounds Bp4mT, Bp4eT, and Bp44mT of 114 ± 6, 138 ± 17, and 156 ± 28% relative to the control following a 3 h incubation at 25 μM. This observation probably reflects their increasing lipophilicity and access to intracellular compartments. The positive control, hydrogen peroxide (50 μM), produced a significant ($p < 0.001$) increase in DCF oxidation to 289 ± 4% of control following a 30 min/37 °C incubation.

The incorporation of halogens to the phenyl group of the parent ligands (except FBpT and FBp44mT) resulted in a significant ($p < 0.01$) increase in DCF fluorescence over both the control and the parent ligand (Figure 6B). In all cases, the iodinated analogues led to the greatest increase in H_2DCF oxidation in each series, with an increase of 220 ± 11, 293 ± 13, 370 ± 21, and 469 ± 39% relative to control medium being observed for IBpT, IBp4mT, IBp4eT, and IBp44mT, respectively. The most active chelators at mediating H_2DCF oxidation were the −Br and −I analogues of Bp4eT and Bp44mT, which increased oxidation to 326−469% of the control and were significantly ($p < 0.01$) more effective than H_2O_2.

The influence of halogenation on the oxidation of H_2DCF by the BpT analogues can be divided into two main effects: (i) incorporation of F (except FBpT), which led to a slight increase in DCF fluorescence relative to the parent analogue, and (ii) incorporation of Cl, Br, or particularly I, which led to a significant ($p < 0.01$) enhancement in DCF fluorescence versus the parent

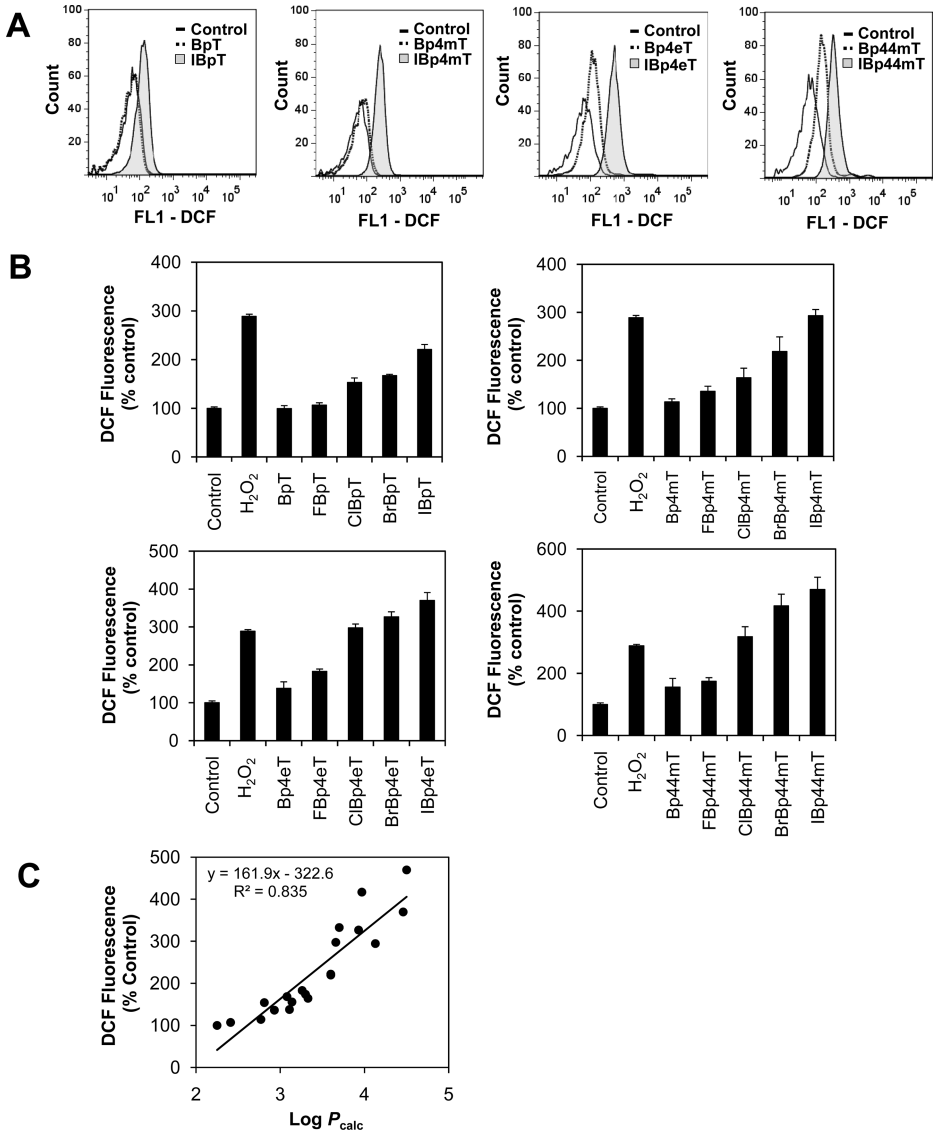

Figure 6. Comparison of the intracellular production of ROS by the parent and XBpT chelators (25 μM) as demonstrated by the oxidation of nonfluorescent H_2DCF to fluorescent DCF following a 3 h incubation at 37 °C. The DCF probe fluorescence was quantified by flow cytometry in SK-N-MC cells. The positive control, H_2O_2 (50 μM), was incubated with cells for 30 min/37 °C. (A) As relative examples of the flow cytometry results, presented are the following: control cells (solid line) or cells incubated with the parent BpT ligand (dashed line) or iodinated BpT ligand (shaded area). (B) Quantification of the flow cytometric results for all examined ligands showing the percentage increase in DCF fluorescence over that observed for control cells. Results are means ± SDs (n = 6). (C) The relationship between DCF fluorescence and lipophilicity (log P_{calcd}).

compound. Plotting these values against the calculated log P_{calcd} of the ligand, we observed a positive linear relationship between DCF fluorescence and lipophilicity for all halogenated analogues examined (Figure 6C). Hence, the enhanced permeability of the chelator due to halogen addition probably plays an important role in the increased intracellular redox activity observed. This factor appears crucial in terms of interpreting these data, as there was little difference in the ability of these analogues to oxidize ascorbate (Figure 5).

Assessment of H_2DCF oxidation as a function of antiproliferative activity (IC_{50}) against SK-N-MC cells revealed a positive correlation between these parameters for the XBpT (r^2 = 0.68) and XBp4mT (r^2 = 0.67) series of halogenated ligands (data not shown). Hence, it can be hypothesized that increasing the lipophilicity of these ligands by halogenation led to ligands entering the optimum lipophilic range (log P_{calcd} 3.1−4.5; Table 1 and Figure 3), which resulted in enhanced permeability, intracellular redox activity (Figure 6), and antiproliferative efficacy (Table 2). However, no such correlation between H_2DCF oxidation as a function of antiproliferative activity was observed for the more lipophilic XBp4eT and XBp44mT series of ligands (r^2 = 0.20 and 0.05, respectively). This lack of relationship for the latter ligands suggests that the already optimal lipophilicity of the parent compounds (i.e., Bp4eT and Bp44mT; Table 1 and Figure 3) meant that while halogenation results in increased intracellular redox activity, this did not potentiate antitumor activity. This may indicate that other factors in addition to a certain threshold of redox activity are essential for the antiproliferative efficacy of the XBp4eT and XBp44mT series. Indeed, it is known that chelators act by multiple

dx.doi.org/10.1021/jm200924c |J. Med. Chem. 2011, 54, 6936–6948

mechanisms to inhibit tumor cell growth, including their effects on molecules involved in DNA synthesis (i.e., ribonucleotide reductase),[9−11] cell cycle progression (i.e., cyclin D1 and p21),[12,14,15] and growth and metastasis suppression (i.e., p53 and NDRG1).[13,15,16]

CONCLUSIONS

The incorporation of a halogen into the phenyl group of the BpT series of ligands generated chelators with potent antiproliferative activity against neoplastic cells. Importantly, an appreciable in vitro therapeutic index was observed as tumor cells were more sensitive to the effects of the chelators than mortal cells. The increased antineoplastic activity of some of the XBpT series can, in part, be attributed to their enhanced lipophilicity due to the presence of a halogen group. This effect was most clearly evident with the more hydrophilic chelators (i.e., XBpT and XBp4mT series), as demonstrated by the fact that the antiproliferative activity of the parent BpT ligand against SK-N-MC cells increased 32-fold by the addition of I (Table 2). The addition of halogens to the more lipophilic parent ligands (i.e., Bp4eT and Bp44mT) led to no marked improvement of antiproliferative activity against tumor cells. Potentially, this latter effect could be because the parent compounds were already sufficiently lipophilic to gain intracellular access to crucial Fe pools and that a further increase in lipophilicity did not enhance this. By examining the library of synthesized compounds, we established that the optimal lipophilic (log P_{calcd}) range was between 3.1 and 4.5, with the greatest antiproliferative efficacy being evident at log $P_{calcd} \sim 4$ (Figure 3). Hence, these latter data support the reasoning above, namely, that halogenation of the BpT and Bp4mT parent ligands led to analogues that approached or were within this optimal lipophilic range, while the lipophilicity of the Bp4eT and Bp44mT parents were already within the optimal range (Table 1).

Generally, the XBpT analogues exhibited a significant ability to mobilize intracellular ^{59}Fe from prelabeled cells and to inhibit ^{59}Fe uptake from the serum Fe-binding protein Tf, being far more effective than the clinically used chelator, DFO. However, in comparison to their respective parent ligands, halogenation led to reduced ^{59}Fe mobilization activity and a decreased ability to inhibit ^{59}Fe uptake from Tf. Hence, increased lipophilicity (log P) within each series led to decreased Fe chelation efficacy (Figure 4). This could possibly reflect accumulation of the ligand or its Fe complex in subcellular organelles or entrapment in cell membranes due to their high affinity for the lipid environment.

The incorporation of a halogen led to a halogen-specific increase in the redox potential of XBpT−Fe complexes. Their higher redox potentials did not appreciably affect their ability to mediate ascorbate oxidation. However, incorporation of Cl, Br, or I significantly enhanced H_2DCF oxidation between 1.5- and 4.7-fold relative to all of the parent analogues. In addition, a positive correlation (r^2 = 0.835) was observed between DCF fluorescence and lipophilicity (log P_{calcd}; Figure 6C). Considering these latter results, the permeability of the chelator appears to be a crucial factor for the higher intracellular redox activity observed using the DCF assay. This is supported by the fact that halogenation of the parent chelators did not significantly affect ascorbate oxidation, where no permeability barrier was involved (i.e., the cell membrane).

Collectively, the current results demonstrate that the addition of halogens to the more hydrophilic XBpT analogues (i.e., XBpT and XBp4mT) increased their lipophilicity into the optimal range (i.e., log P_{calcd} 3.1−4.5; Table 1 and Figure 3A,B), leading to increased intracellular redox activity and antiproliferative efficacy. In contrast, the addition of halogens to the more lipophilic XBp4eT and XBp44mT analogues resulted in no correlation between intracellular redox activity and antiproliferative efficacy, despite the increase in H_2DCF oxidation. This was probably because the lipophilicity of the parent compound was already within the optimal range (Table 1 and Figure 3A,B), with a further increase due to halogenation not resulting in a substantial benefit to antiproliferative activity.

EXPERIMENTAL PROCEDURES

All commercial reagents were used without further purification. DFO was obtained from Novartis (Basel, Switzerland). The 2-(4-halobenzoyl)pyridines were obtained from Rieke Metals Inc. (Lincoln, United States). The chelators, Dp44mT and NIH, were prepared and characterized according to previously described methods.[31,35] Combustion analysis (C, H, N) of the ligands and complexes was performed to confirm ≥95% purity.

Chelators of the XBpT Series: General Synthesis. The ligands were synthesized by the following general procedure: 2-(4-Halobenzoyl)pyridine (0.01 mol) was dissolved in 15 mL of ethanol/methanol, and subsequently, 1.00 g (0.01 mol) of the appropriate thiosemicarbazide was dissolved in warm water (15 mL), and the two solutions were then mixed. Glacial acetic acid (5−6 drops) was added, and the mixture was gently refluxed for 2−5 h. The mixture was cooled to room temperature and allowed to stand in a refrigerator overnight to ensure complete precipitation. The product was filtered off and washed with ethanol (10 mL) followed by diethyl ether (10 mL).

FBpT. Yield, 77%. Anal. calcd for $C_{13}H_{11}N_4SF$: C, 56.92%; H, 4.04%; N, 20.42%. Found: C, 56.31%; H, 4.09%; N, 19.77%. ^{1}H NMR (DMSO-d_6): 8.67 (dq, 1H), 8.15 (dq, 1H), 8.39 (s, 1H), 8.05 (dd, 1H), 7.97−7.54 (m, 3H), 7.45−7.33 (dt, 3H). IR (cm^{-1}): 3391w, 3290m, 3151w, 3057w, 1640w, 1587s, 1509s, 1478s, 1421m, 1362w, 1329m, 1255m, 1223m, 1159m, 1108s, 1090m, 1057w, 1047w, 999w, 942w, 851s, 835s, 799m, 740m, 659m, 623m, 604m, 586m, 563m. MS (EI) m/z 274 (M$^+$).

ClBpT.CH$_3$OH. Yield, 82%. Anal. calcd for $C_{14}H_{15}N_4OSCl$: C, 52.09%; H, 4.68%; N, 17.36%. Found: C, 52.41%; H, 4.67%; N, 17.60%. ^{1}H NMR (DMSO-d_6): 8.53 (dq, 1H), 8.22 (dq, 1H), 8.39 (s, 1H), 8.05 (dd, 1H), 7.87−7.44 (m, 3H), 7.40−7.23 (dt, 3H). IR (cm^{-1}): 3393w, 3276m, 3130w, 3096w, 1620w, 1590s, 1551w, 1473s, 1421m, 1397w, 1326m, 1256m, 1158w, 1108s, 1089s, 1065w, 1050w, 1014m, 949w, 854s, 827s, 796m, 779w, 734w, 678w, 657w, 633w, 620w, 598m, 523s. MS (EI) m/z 290 (M$^+$).

BrBpT. Yield, 85%. Anal. calcd for $C_{13}H_{11}N_4SBr$: C, 46.58%; H, 3.31%; N, 16.71%. Found: C, 46.1%; H, 3.16%; N, 16.36%. ^{1}H NMR (DMSO-d_6): 8.63 (dq, 1H), 8.22 (dq, 1H), 8.43 (s, 1H), 8.23 (dd, 1H), 7.90−7.54 (m, 3H), 7.43−7.29 (dt, 3H). IR (cm^{-1}): 3405w, 3277m, 3155w, 3096w, 1620w, 1590s, 1539w, 1473s, 1421s, 1391w, 1327m, 1257w, 1178w, 1158w, 1108s, 1089s, 1070w, 1050w, 1009m, 948w, 854s, 825s, 796m, 750w, 729w, 720w, 690w, 656w, 620w, 598m, 523m. MS (EI) m/z 335 (M$^+$).

IBpT·1/2H$_2$O. Yield, 92%. Anal. calcd for $C_{13}H_{13}N_4OSI$: C, 39.91%; H, 3.09%; N, 14.30%. Found: C, 39.83%; H, 2.89%; N, 14.00%. IR (cm^{-1}): 3416w, 3295m, 3156w, 1620w, 1588s, 1535w, 1472s, 1421m, 1388w, 1365w, 1326m, 1256w, 1170w, 1107m, 1088m, 1005m, 962w, 948w, 853s, 823m, 794m, 748w, 713w, 682w, 655w, 632w, 620w, 597m, 520m, 492m. ^{1}H NMR (DMSO-d_6): 8.53 (dq, 1H), 8.22 (dq, 1H), 8.33 (s, 1H), 8.51 (dd, 1H), 7.80−7.54 (m, 3H), 7.33−7.29 (dt, 3H). MS (EI) m/z 382 (M$^+$).

FBp4mT·1/2H$_2$O. Yield, 79%. Anal. calcd for $C_{14}H_{14}N_4O_{0.5}SF$: C, 56.55%; H, 4.75%; N, 18.84%. Found: C, 55.96%; H, 4.52%; N, 18.60%.

^{1}H NMR (DMSO-d_6): 8.75 (d, 1H, pyr), 8.61 (d, 1H, pyr), 8.21 (t, 1H, pyr), 7.53 (m, 3H, pyr), 7.15 (m, 3H, pyr), 7.21 (m, 1H, pyr), 3.04 (d, 3H,-CH_3). IR (cm^{-1}): 3307 m, 3146w, 2940w, 1601m, 1541s, 1509m, 1482s, 1452m, 1407m, 1360w, 1314m, 1226s, 1159m, 1113m, 1095m, 1047m, 996w, 942w, 845m, 814m, 797m, 735m, 663m, 648m, 620w, 592m, 511m. MS (EI) m/z 288 (M$^+$).

ClBp4mT·H$_2$O. Yield, 81%. Anal. calcd for $C_{14}H_{15}N_4OSCl$: C, 52.09%; H, 4.68%; N, 17.36%. Found: C, 52.71%; H, 4.11%; N, 17.57%. ^{1}H NMR (DMSO-d_6): 8.63 (d, 1H, pyr), 8.52 (d, 1H, pyr), 8.16 (t, 1H, pyr), 7.33 (m, 3H, pyr), 7.09 (m, 3H, pyr), 7.41 (m, 1H, pyr), 3.14 (d, 3H,-CH_3). IR (cm^{-1}): 3357m, 3124w, 3054w, 1580m, 1548s, 1480s, 1427m, 1397m, 1369w, 1312m, 1269w, 1235s, 1161w, 1115m, 1105m, 1089m, 1039m, 1011w, 950w, 835s, 820m, 800w, 775w, 751w, 721w, 655w, 639m, 621m, 576m. MS (EI) m/z 304 (M$^+$).

BrBp4mT·1/2H$_2$O. Yield, 83%. Anal. calcd for $C_{14}H_{14}N_4O_{0.5}SBr$: C, 46.94%; H, 3.94%; N, 15.64%. Found: C, 46.5%; H, 3.50%, N, 15.50%. ^{1}H NMR (DMSO-d_6): 8.43 (d, 1H, pyr), 8.22 (d, 1H, pyr), 8.16 (t, 1H, pyr), 7.33 (m, 3H, pyr), 7.11 (m, 3H, pyr), 7.56 (m, 1H, pyr), 3.08 (d, 3H,-CH_3). IR (cm^{-1}): 3357m, 3124w, 3054w, 1590m, 1548s, 1480s, 1427m, 1397m, 1369w, 1312m, 1269w, 1235s, 1161w, 1114m, 1105m, 1089m, 1039m, 1010w, 950w, 835s, 820m, 801w, 775w, 751w, 721w, 655w, 639m, 621m, 576m. MS (EI) m/z 348 (M$^+$).

IBp4mT·1/2H$_2$O. Yield, 88%. Anal. calcd for $C_{14}H_{14}N_4O_{0.5}SI$: C, 41.49%; H, 3.48%; N, 13.83%. Found: C, 41.34%; H, 3.16% N, 13.69%. ^{1}H NMR (DMSO-d_6): 8.54 (d, 1H, pyr), 8.13 (d, 1H, pyr), 8.19 (t, 1H, pyr), 7.33 (m, 3H, pyr), 7.23 (m, 3H, pyr), 7.44 (m, 1H, pyr), 3.10 (d, 3H,-CH_3). IR (cm^{-1}): 3357m, 3124w, 3054w, 1595m, 1548s, 1480s, 1427m, 1397m, 1364w, 1312m, 1269w, 1235s, 1161w, 1112w, 1100w, 1089m, 1039m, 1011w, 950w, 836m, 820m, 800w, 775w, 750w, 721w, 639w, 621w, 576m, 498m. MS (EI) m/z 396 (M$^+$).

FBp4eT. Yield, 94%. Anal. calcd for $C_{15}H_{15}N_4SF$: C, 59.58%; H, 5.00%; N, 18.53%. Found: C, 59.63%; H, 4.99%; N, 18.40%. ^{1}H NMR (DMSO-d_6): 8.55 (t, 1H), 8.05 (td, 1H), 7.73−7.66 (td, 1H), 7.47−7.42 (m, 3H), 7.34 (dt, 1H), 3.65 (m, 2H), 1.06 (t, 3H). IR (cm^{-1}): 3282m, 3090w, 2977w, 2937w, 1599m, 1541s, 1475s, 1433m, 1420m, 1371w, 1310s, 1218s, 1155m, 1113m, 1094w, 1052m, 1001w, 931m, 848s, 813m, 794m, 738s, 682m, 658m, 621w, 452m. MS (EI) m/z 302 (M$^+$).

ClBp4eT·1/2H$_2$O. Yield, 93%. Anal. calcd for $C_{15}H_{16}N_4O_{0.5}SCl$: C, 54.96%; H, 4.92%; N, 17.09%; S, 9.78%. Found: C, 55.38%; H, 4.78%; N, 17.53; S, 9.47%. IR (cm^{-1}): 3303m, 3100w, 2965w, 2935w, 1585m, 1536s, 1479s, 1432m, 1310s, 1251w, 1217s, 1154w, 1114m, 1091m, 1055m, 1013w, 930w, 846m, 811m, 794m, 745m, 676m, 658w, 621w, 501s. ^{1}H NMR (DMSO-d_6): 8.55 (t, 1H), 8.05 (td, 1H), 7.73−7.66 (td, 1H), 7.47−7.42 (m, 3H), 7.34 (dt, 1H), 3.65 (m, 2H), 1.06 (t, 3H). MS (EI) m/z 318 (M$^+$).

BrBp4eT·1/2H$_2$O. Yield, 91%. Anal. calcd for $C_{15}H_{16}N_4O_{0.5}SBr$: C, 48.39%; H, 4.33%; N, 15.05%; S, 8.61%. Found: C, 47.93%; H, 4.05%; N, 14.87%; S, 8.35%. ^{1}H NMR (DMSO-d_6): 8.51 (t, 1H), 8.33 (td, 1H), 7.80−7.56 (td, 1H), 7.47−7.33 (m, 3H), 7.24 (dt, 1H), 3.55 (m, 2H), 1.08 (t, 3H). IR (cm^{-1}): 3277mw, 3114w, 2970w, 2929w, 1591m, 1532s, 1471s, 1420m, 1392w, 1310s, 1252w, 1216s, 1151w, 1115m, 1053m, 1011w, 928w, 835m, 811w, 796w, 777w, 737m, 654w, 619w, 498w. MS (EI) m/z 364 (M$^+$).

IBp4eT·1/2H$_2$O. Yield, 94%. Anal. calcd for $C_{15}H_{16}N_4O_{0.5}SI$: C, 42.97%; H, 3.85%; N, 13.36%. Found: C, 43.05%; H, 3.57%; N, 13.33%. ^{1}H NMR (DMSO-d_6): 8.44 (t, 1H), 8.22 (td, 1H), 7.76−7.56 (td, 1H), 7.41−7.32 (m, 3H), 7.28 (dt, 1H), 3.34 (m, 2H), 1.08 (t, 3H). IR (cm^{-1}): 3284m, 3168w, 3078w, 2972w, 2929w, 1587m, 1533s, 1469s, 1421m, 1368m, 1310s, 1251w, 1216s, 1194s, 1150w, 1114m, 1098m, 1058m, 1007m, 955w, 928m, 830m, 809m, 798w, 777w, 736m, 676w, 617w, 494m. MS (EI) m/z 410 (M$^+$).

FBp44mT. Yield, 96%. Anal. calcd for $C_{15}H_{15}N_4SF$: C, 59.58%; H, 5.00%; N, 18.53%. Found: C, 59.93%; H, 4.99%; N, 18.30%. ^{1}H NMR (DMSO-d_6): 8.70 (dd, 1H), 8.45 (dd, 1H), 8.12−7.84 (dd, 2H), 7.66−7.44 (dd, 4H), 7.33 (dt, 1H), 3.35 (s, 3H), 3.25 (s, 3H). IR (cm^{-1}): 3059m, 2925w, 1587m, 1541s, 1506s, 1461s, 1424m, 1371m, 1314s, 1234s, 1154s, 1118s, 1065m, 1005m, 966m, 908s, 835s, 794m, 723s, 699m, 658w, 612w, 581m, 494m. MS (EI) m/z 302 (M$^+$).

ClBp44mT·1/2H$_2$O. Yield, 90%. Anal. calcd for $C_{15}H_{16}N_4O_{0.5}SCl$: C, 54.96%; H, 4.92%; N, 17.09%; S, 9.78%. Found: C, 55.22%; H, 4.65%; N, 17.49%; S, 9.77%. ^{1}H NMR (DMSO-d_6): 8.70 (dd, 1H), 8.46 (dd, 1H), 8.12−7.84 (dd, 2H), 7.66−7.44 (dd, 4H), 7.33 (dt, 1H), 3.35 (s, 3H), 3.25 (s, 3H). IR (cm^{-1}): 3058m, 2925w, 1585m, 1541s, 1506s, 1460m, 1424w, 1371m, 1314s, 1234s, 1154s, 1118s, 1065m, 1005m, 966m, 909s, 835s, 795m, 723s, 699m, 658w, 611w, 581w. MS (EI) m/z 318 (M$^+$).

BrBp44mT·1/2H$_2$O. Yield, 95%. Anal. calcd for $C_{15}H_{16}N_4O_{0.5}SBr$: C, 48.39%; H, 4.33%; N, 15.05%; S, 8.61%. Found: C, 48.31%; H, 3.96%; N, 15.27%; S, 8.53%. ^{1}H NMR (DMSO-d_6): 8.69 (dd, 1H), 8.50 (dd,1H), 8.27−7.81 (dd, 2H), 7.63−7.58 (dd, 4H), 7.44 (dt, 1H), 3.25 (s, 3H), 3.13 (s, 3H). IR (cm^{-1}): 3080w, 2940w, 1586m, 1537s, 1487m, 1465w, 1445w, 1374s, 1333s, 1310s, 1229s, 1176s, 1122s, 1068m, 1009m, 962m, 907m, 834s, 797s, 747m, 690w, 650m, 606w, 446w. MS (EI) m/z 363 (M$^+$).

IBp44mT. Yield, 96%. Anal. calcd. for $C_{15}H_{15}N_4SI$: C, 43.91%; H, 3.68%; N, 13.66%; S, 7.81%. Found: C, 43.53%; H, 3.56%; N, 13.39%; S, 7.88%. ^{1}H NMR (DMSO-d_6): 8.66 (dd, 1H), 8.32 (dd,1H), 8.22−7.89 (dd, 2H), 7.33−7.55 (dd, 4H), 7.44 (dt, 1H), 3.25 (s, 3H), 3.13 (s, 3H). IR (cm^{-1}): 3060w, 2931w, 1584m, 1533s, 1506m, 1446w, 1375s, 1330s, 1313s, 1228s, 1169m, 1117s, 1060m, 1008m, 958m, 908m, 839s, 803m, 778m, 733m, 655m, 611w, 492w. MS (EI) m/z 410 (M$^+$).

General Synthesis of [Fe^{III}(XBpT)]$^+$ Complexes. The iron complexes were prepared by the following general method. The appropriate thiosemicarbazone (3.5 mmol) was dissolved in 15 mL of ethanol. Minimal amounts of MeCN were added dropwise to aid dissolution. Once dissolved, 0.36 g of Et_3N was added to the solution. Then, 0.81 g (1.7 mmol) of $Fe(ClO_4)_3·6H_2O$ was added, and the mixture was gently refluxed for 60 min. After it was cooled, the dark brown powder was filtered off and washed with ethanol (10 mL) followed by diethyl ether (10 mL).

[Fe(FBpT)$_2$]ClO$_4$·3H$_2$O. Yield, 33%. Anal. calcd for $C_{26}H_{26}ClFeN_8O_7S_2F_2$: C, 41.31%; H, 3.47%; N, 14.82%. Found: C, 41.10%; H, 3.71%; N, 14.50%. IR (cm^{-1}): 3308w, 1602s, 1506s, 1482s, 1433s, 1324s, 1228s, 1208s, 1146s, 1092s, 956w, 851m, 784s, 755m, 720m, 650m, 627s.

[Fe(ClBpT)$_2$]ClO$_4$·CH$_3$CH$_2$OH. Yield, 37%. Anal. calcd for $C_{28}H_{25}Cl_3FeN_8O_5S_2$: C, 43.07%; H, 3.36%; N, 14.35%; S, 8.21%. Found: C, 42.7%; H, 4.05%; N, 14.34%; S, 7.89%. IR (cm^{-1}): 3274w, 1591s, 1493s, 1471s, 1443s, 1422s, 1326s, 1227m, 1147s, 1107s, 1089s, 1014s, 854s, 828s, 797s, 705w, 651w, 624s.

[Fe(BrBpT)$_2$]ClO$_4$·H$_2$O. Yield, 38%. Anal. calcd for $C_{26}H_{22}ClFeN_8O_5S_2Br_2$: C, 37.10%; H, 2.63%; N, 13.31%; S, 7.62%. Found: C, 36.90%; H, 2.55%; N, 13.19%; S, 7.59%. IR (cm^{-1}): 3279w, 1610s, 1590s, 1493s, 1424vs, 1322s, 1207s, 1147s, 1104s, 1011s, 942m, 853m, 840m, 830m, 797s, 747s, 728w, 655s, 624s.

[Fe(IBpT)$_2$]ClO$_4$·2CH$_3$CN. Yield, 39%. Anal. calcd for $C_{32}H_{29}ClFeN_{11}O_4S_2I_2$: C, 36.04%; H, 2.62%; N, 14.01%. Found: C, 36.18%; H, 2.72%; N, 13.62%. IR (cm^{-1}): 3354w, 1608s, 1592s, 1492s, 1428vs, 1320s, 1207s, 1144s, 1092vs, 1007s, 943w, 852s, 797s, 748w, 726w, 624s.

[Fe(FBp4mT)$_2$]ClO$_4$. Yield, 37%. Anal. calcd for $C_{28}H_{24}ClFeN_8O_4S_2F_2$: C, 46.07%; H, 3.31%; N, 15.35%; S, 8.78%. Found: C, 46.06%; H, 3.13%; N, 15.59%; S, 8.93%. IR (cm^{-1}): 3383w, 1602w, 1548s, 1519s, 1495s, 1449s, 1400s, 1338s, 1297s, 1269s, 1234s, 1204s, 1161s, 1104vs, 970w, 850m, 834m, 785s, 756w, 623s.

[Fe(ClBp4mT)$_2$]ClO$_4$. Yield, 41%. Anal. calcd for $C_{28}H_{24}Cl_3FeN_8O_4S_2$: C, 44.08%; H, 3.17%; N, 14.69%; S, 8.41%. Found: C, 44.11%; H, 3.17%; N, 14.85%; S, 8.48%. IR (cm^{-1}): 3392w, 1594w, 1548s, 1509s, 1448s, 1403s, 1335s, 1297w, 1267s, 1204s, 1164s, 1091vs, 1015w, 969w, 841m, 809w, 785m, 756w, 723w, 623s.

[Fe(BrBp4mT)$_2$]ClO$_4$. Yield, 42%. Anal. calcd for $C_{28}H_{24}ClFeN_8O_4S_2Br_2$: C, 39.48%; H, 2.84%; N, 13.16%; S, 7.53%. Found: C, 39.60%; H, 2.91%; N, 13.40%; S, 7.38%. IR (cm^{-1}): 3396w, 1588w, 1545s, 1508s, 1447s, 1402s, 1333s, 1297w, 1267s, 1204s, 1164s, 1092vs, 1012m, 968m, 839m, 807w, 785m, 756w, 718w, 622s.

[Fe(IBp4mT)$_2$]ClO$_4$·CH$_3$CN. Yield, 44%. Anal. calcd for $C_{30}H_{27}ClFeN_9O_4S_2I_2$: C, 36.51%; H, 2.76%; N, 12.77%; S, 6.50%. Found: C, 36.69%; H, 2.47%; N, 12.28%; S, 6.72%. IR (cm^{-1}): 3394w, 1587w, 1544s, 1505s, 1447s, 1400s, 1332s, 1297w, 1266s, 1204s, 1163m, 1088vs, 1007s, 967m, 837w, 806w, 784m, 755w, 717w, 622s.

[Fe(FBp4eT)$_2$]ClO$_4$. Yield, 31%. Anal. calcd for $C_{30}H_{28}ClFeN_8O_4S_2F_2$: C, 47.54%; H, 3.72%; N, 14.78%; S, 8.46%. Found: C, 47.63%; H, 3.71%; N, 14.50%; S, 8.14%. IR (cm^{-1}): 3383w, 1602w, 1543s, 1517s, 1493s, 1427s, 1334s, 1299s, 1266s, 1238s, 1198m, 1160s, 1094vs, 960w, 850m, 834m, 783s, 751w, 625s.

[Fe(ClBp4eT)$_2$]ClO$_4$·CH$_3$CN. Yield, 36%. Anal. calcd for $C_{30}H_{28}Cl_3FeN_8O_4S_2$: C, 46.20%; H, 3.76%; N, 15.15%. Found: C, 46.16%; H, 3.73%; N, 14.90%. IR (cm^{-1}): 3401w, 1593w, 1540s, 1506s, 1493s, 1422s, 1331s, 1295s, 1261s, 1197m, 1153s, 1091vs, 1014m, 968w, 840w, 802w, 752w, 623s.

[Fe(BrBp4eT)$_2$]ClO$_4$·CH$_3$CN. Yield, 40%. Anal. calcd for $C_{32}H_{31}ClFeN_9O_4S_2Br_2$: C, 41.74%; H, 3.39%; N, 13.69%; S, 6.96%. Found: C, 41.80%; H, 3.77%; N, 13.97%; S, 7.17%. 3398w, 1586w, 1535s, 1504s, 1473s, 1423s, 1332s, 1308s, 1216m, 1150s, 1115vs, 1012s, 968w, 836m, 797w, 737w, 621s.

[Fe(IBp4eT)$_2$]ClO$_4$. Yield, 42%. Anal. calcd for $C_{32}H_{29}ClFeN_{11}O_4S_2I_2$: C, 37.00%; H, 3.77%; N, 11.51%; S, 6.58%. Found: C, 37.16%; H, 3.72%; N, 11.63%; S, 6.49%. IR (cm^{-1}): 3357w, 1595w, 1541s, 1502s, 1475m, 1440s, 1331s, 1294s, 1262s, 1196s, 1149s, 1100vs, 1008s, 968m, 835w, 802w, 780w, 754w, 716w, 622s.

[Fe(FBp44mT)$_2$]ClO$_4$·CH$_3$CN. Yield, 28%. Anal. calcd for $C_{32}H_{31}ClFeN_9O_4S_2F_2$: C, 48.10%; H, 3.91%; N, 15.78%; S, 8.02%. Found: C, 47.87%; H, 3.63%; N, 15.40%; S, 8.09%. IR (cm^{-1}): 2938w, 1602w, 1543s, 1510s, 1460s, 1437s, 1394s, 1345s, 1302s, 1263, 1205s, 1154w, 1094vs, 977w, 920s, 783m, 748w, 723m, 692s, 663w, 633w, 620s.

[Fe(ClBp44mT)$_2$]ClO$_4$. Yield, 38%. Anal. calcd for $C_{30}H_{28}Cl_3FeN_8O_4S_2$: C, 45.56%; H, 3.57%; N, 14.17%; S, 8.11%. Found: C, 45.53%; H, 3.49%; N, 14.21%; S, 8.44%. IR (cm^{-1}): 2936w, 1599w, 1542s, 1508s, 1461s, 1437s, 1395s, 1345s, 1302s, 1263, 1207s, 1154w, 1091vs, 978w, 921s, 781m, 748m, 725w, 792s, 663w, 632w, 622s.

[Fe(BrBp44mT)$_2$]ClO$_4$. Yield, 43%. Anal. calcd for $C_{30}H_{28}ClFeN_8O_4S_2Br_2$: C, 40.95%; H, 3.21%; N, 12.74%; S, 7.29%. Found: C, 41.22%; H, 3.38%; N, 12.33%; S, 7.24%. IR (cm^{-1}): 2937w, 1600w, 1541s, 1510s, 1463s, 1436s, 1393s, 1345s, 1302s, 1260, 1210s, 1151w, 1092vs, 978w, 922s, 781m, 748w, 724m, 690s, 663w, 632w, 622s.

[Fe(IBp44mT)$_2$]ClO$_4$. Yield, 42%. Anal. calcd for $C_{30}H_{28}ClFeN_8O_4S_2I_2$: C, 37.00%; H, 2.90%; N, 11.51%; S, 6.58%. Found: C, 37.44%; H, 2.99%; N, 11.83%; S, 6.89%. IR (cm^{-1}): 2912w, 1589w, 1542s, 1505s, 1473s, 1436s, 1383s, 1346s, 1302s, 1262, 1210s, 1149m, 1099vs, 974w, 922s, 780w, 752w, 720m, 681s, 662w, 632w, 622s.

Physical Methods. ^{1}H NMR (400 MHz) spectra were acquired using a Bruker Avance 400 NMR spectrometer with DMSO-d_6 as the solvent and internal reference (Me_2SO: ^{1}H NMR δ 2.49 ppm and ^{13}C NMR δ 39.5 ppm vs TMS). Infrared spectra were measured with a Varian Scimitar 800 FT-IR spectrophotometer with compounds being dispersed as KBr discs. Cyclic voltammetry was performed using a BAS100B/W potentiostat. A glassy carbon working electrode, an aqueous Ag/AgCl reference, and a Pt wire auxiliary electrode were used. All complexes were at ca. 1 mM concentration in MeCN:H_2O 70:30 v/v. This solvent combination was used to ensure solubility of all compounds. The supporting electrolyte was Et_4NClO_4 (0.1 M), and the solutions were purged with nitrogen prior to measurement. All potentials are cited versus the normal hydrogen electrode (NHE) by addition of 196 mV to the potentials measured relative to the Ag/AgCl reference. Partition coefficients of the free ligands were determined by ChemBioDraw v.11.0.1. (CambridgeSoft) using Crippen's fragmentation procedure.[42]

Crystallography. Intensity data were acquired on an Oxford Diffraction Gemini Ultra S CCD diffractometer. Data reduction was performed with the CrysAlisPro program (version 171.33.42). The structures were solved by direct methods with SHELX-86 and refined by full matrix least-squares with SHELXL.[43] Thermal ellipsoid diagrams were generated with ORTEP3.[44] All calculations were carried out within the WinGX package.[45]

Biological Studies. *Cell Culture.* Chelators were dissolved in DMSO as 10 mM stock solutions and diluted in medium containing 10% fetal calf serum (Commonwealth Serum Laboratories, Melbourne, Australia) so that the final [DMSO] < 0.5% (v/v). At this final concentration, DMSO had no effect on proliferation, ^{59}Fe uptake, or ^{59}Fe mobilization from cells, as shown previously.[37] The human SK-N-MC neuroepithelioma cell line and mortal human MRC5 fibroblasts (American Type Culture Collection, Manassas, VA) were grown by standard procedures[37] at 37 °C in a humidified atmosphere of 5% CO_2/95% air in an incubator (Forma Scientific, Marietta, OH).

Effect of the Chelators on Cellular Proliferation. The effect of the chelators and complexes on cellular proliferation was determined by the [1-(4,5-dimethylthiazol-2-yl)-2,5-diphenyl tetrazolium] (MTT) assay using standard techniques.[37,46] The SK-N-MC cell line was seeded in 96-well microtiter plates at 1.5×10^4 cells/well in medium containing human $^{56}Fe_2$-Tf (1.25 μM) and chelators at a range of concentrations (0−25 μM). Control samples contained medium with Fe_2-Tf (1.25 μM) without the ligands. The cells were incubated at 37 °C in a humidified atmosphere containing 5% CO_2 and 95% air for 72 h. After this incubation, 10 μL of MTT (5 mg/mL) was added to each well and further incubated at 37 °C/2 h. After solubilization of the cells with 100 μL of 10% SDS-50% isobutanol in 10 mM HCl, the plates were read at 570 nm using a scanning multiwell spectrophotometer. The inhibitory concentration (IC_{50}) was defined as the chelator concentration necessary to reduce the absorbance to 50% of the untreated control. Using this method, absorbance was shown to be directly proportional to cell counts, as shown previously.[37]

Preparation of ^{56}Fe- and ^{59}Fe-Tf. Human Tf (Sigma) was labeled with ^{56}Fe or ^{59}Fe (Dupont NEN, MA) to produce $^{59}Fe_2$-Tf and $^{56}Fe_2$-Tf, respectively, as previously described.[39,46] Unbound ^{59}Fe was removed by passage through a Sephadex G25 column and exhaustive vacuum dialysis against a large excess of 0.15 M NaCl buffered to pH 7.4 with 1.4% $NaHCO_3$ by standard methods.[46]

Effect of Chelators on ^{59}Fe Efflux from Cells. Iron efflux experiments examining the ability of various chelators to mobilize ^{59}Fe from SK-N-MC cells were performed using established techniques.[37,47] Briefly, following prelabeling of cells with $^{59}Fe_2$-Tf (0.75 μM) for 3 h/37 °C, the cell cultures were washed on ice four times with ice-cold PBS and then subsequently incubated with each chelator (25 μM) for 3 h/37 °C. The overlying media containing released ^{59}Fe was then separated from the cells using a Pasteur pipet. The radioactivity was measured in both the cell pellet and the supernatant using a γ-scintillation counter (Wallac Wizard 3, Turku, Finland). In these studies, the novel ligands were compared to the previously characterized chelators, DFO, NIH, and Dp44mT.

Effect of Chelators at Preventing ^{59}Fe Uptake from $^{59}Fe_2$-Tf by Cells. The ability of the chelator to prevent cellular ^{59}Fe uptake from the serum Fe transport protein, $^{59}Fe_2$-Tf, was examined using established techniques.[18,48] Briefly, cells were incubated with $^{59}Fe_2$-Tf (0.75 μM) for 3 h/37 °C in the presence of each of the chelators (25 μM). The cells were then washed four times with ice-cold PBS, and internalized ^{59}Fe was determined by standard techniques by incubating the cell monolayer for 30 min/4 °C with the general protease, Pronase (1 mg/mL; Sigma).[37,49,50] The cells were removed from the monolayer using a plastic spatula and centrifuged at 14000 rpm/1 min. The supernatant

represents membrane-bound, Pronase-sensitive ^{59}Fe that was released by the protease, while the Pronase-insensitive fraction represents internalized ^{59}Fe.[49,50] The novel ligands were compared to the previously characterized chelators, DFO, NIH, and Dp44mT.

Ascorbate Oxidation Assay. An established protocol was used to measure ascorbate oxidation.[2,9,51] Briefly, ascorbic acid (100 μM) was prepared immediately prior to an experiment and incubated in the presence of Fe^{III} (10 μM; added as $FeCl_3$), a 50-fold molar excess of citrate (500 μM), and the chelator (1−60 μM). The absorbance at 265 nm was measured after 10 and 40 min at room temperature, and the decrease of intensity between these time points was calculated.[40] The results of these experiments were expressed in terms of IBEs due to the varying denticity of the chelators examined.

Intracellular ROS Measurements. Intracellular ROS generation was measured using H_2DCF-DA.[18,41] H_2DCF-DA is hydrolyzed by intracellular esterases to H_2DCF, which leads to it becoming trapped within the cytosol. Cellular oxidants localized to the cytosol oxidize nonfluorescent H_2DCF to the fluorescent product, DCF.[18,41] SK-N-MC cells were incubated with 30 nM H_2DCF-DA for 30 min/37 °C and then washed twice with ice-cold PBS. The cells were then treated with either the positive control, H_2O_2 (50 μM) for 30 min/37 °C, or a chelator (25 μM) for 3 h/37 °C. Cells were collected for flow cytometric assessment, and intracellular ROS was detected as an increase in green cytosolic DCF fluorescence using a FACS Canto flow cytometer (Becton Dickinson, Lincoln Park, NJ). In these studies, 10000 events were acquired for every sample. Data analysis was performed using FlowJo software v7.5.5 (Tree Star Inc., Ashland, OR).

Statistical Analysis. Experimental data were compared using Student's *t* test. Results were expressed as means ± SDs (number of experiments) and considered to be statistically significant when $p < 0.05$.

■ ASSOCIATED CONTENT

Supporting Information. Crystal data, selected bond lengths, and crystal structures of XBp44mT ligands and their Fe complexes. This material is available free of charge via the Internet at http://pubs.acs.org.

■ AUTHOR INFORMATION

Corresponding Author

*Tel: +61-2-9036-6548. Fax: +61-2-9036-6549. E-mail: d.richardson@med.usyd.edu.au.

■ ACKNOWLEDGMENT

Financial support from the National Health and Medical Research Council (Senior Principal Research Fellowship and Project Grants to D.R.R.) and Australian Research Council (DP0773027 to P.V.B. and D.R.R. and DP1096029 to P.V.B.) is gratefully acknowledged. P.J.J. (10/CDF/2-15) and D.S.K. (08/ECF/1-30) thank the Cancer Institute NSW for Fellowship support. C.S. is the grateful recipient of an Australian Postgraduate Award from the University of Sydney.

■ ABBREVIATIONS USED

3-AP, 3-aminopyridine-2-carboxaldehyde thiosemicarbazone; DCF, 2′,7′-dichlorofluorescein; DFO, desferrioxamine; BpT, 2′-benzoylpyridine thiosemicarbazone; Bp4mT, 2′-benzoylpyridine 4-methyl-3-thiosemicarbazone; Bp4eT, 2′-benzoylpyridine 4-ethyl-3-thiosemicarbazone; Bp44mT, 2′-benzoylpyridine 4,4-dimethyl-3-thiosemicarbazone; DpT, di-2′-pyridylketone thiosemicarbazone; Dp44mT, di-2′-pyridylketone 4,4-dimethyl-3-thiosemicarbazone; H_2DCF, 2′,7′-dichlorodihydrofluorescein; IBE, iron-binding equivalent; XBpT, 2′-(4″-halobenzoyl)pyridine thiosemicarbazone; XBp4mT, 2′-(4″-halobenzoyl)pyridine 4-methyl-3-thiosemicarbazone; XBp4eT, 2′-(4″-halobenzoyl)pyridine 4-ethyl-3-thiosemicarbazone; XBp44mT, 2′-(4″-halobenzoyl)-pyridine 4,4-dimethyl-3-thiosemicarbazone; NIH, 2-hydroxy-1-naphthaldehyde isonicotinoyl hydrazone; ROS, reactive oxygen species; Tf, transferrin

■ REFERENCES

(1) Bergeron, R. J.; Huang, G. F.; Weimar, W. R.; Smith, R. E.; Wiegand, J.; McManis, J. S. Desferrithiocin analogue based hexacoordinate iron(III) chelators. *J. Med. Chem.* **2003**, *46*, 16–24.

(2) Bergeron, R. J.; Wiegand, J.; McManis, J. S.; Bussenius, J.; Smith, R. E.; Weimar, W. R. Methoxylation of desazadesferrithiocin analogues: Enhanced iron clearing efficiency. *J. Med. Chem.* **2003**, *46*, 1470–1477.

(3) Chua, A. C. G.; Ingram, H. A.; Raymond, K. N.; Baker, E. Multidentate pyridinones inhibit the metabolism of nontransferrin-bound iron by hepatocytes and hepatoma cells. *Eur. J. Biochem.* **2003**, *270*, 1689–1698.

(4) Liu, J.; Obando, D.; Schipanski, L. G.; Groebler, L. K.; Witting, P. K.; Kalinowski, D. S.; Richardson, D. R.; Codd, R. Conjugates of desferrioxamine B (DFOB) with derivatives of adamantane or with orally available chelators as potential agents for treating iron overload. *J. Med. Chem.* **2010**, *53*, 1370–1382.

(5) Buss, J. L.; Torti, F. M.; Torti, S. V. The role of iron chelation in cancer therapy. *Curr. Med. Chem.* **2003**, *10*, 1021–1034.

(6) Torti, S. V.; Torti, F. M.; Whitman, S. P.; Brechbiel, M. W.; Park, G.; Planalp, R. P. Tumor cell cytotoxicity of a novel metal chelator. *Blood* **1998**, *92*, 1384–1389.

(7) Turner, J.; Koumenis, C.; Kute, T. E.; Planalp, R. P.; Brechbiel, M. W.; Beardsley, D.; Cody, B.; Brown, K. D.; Torti, F. M.; Torti, S. V. Tachpyridine, a metal chelator, induces G(2) cell-cycle arrest, activates checkpoint kinases, and sensitizes cells to ionizing radiation. *Blood* **2005**, *106*, 3191–3199.

(8) Larrick, J. W.; Cresswell, P. Modulation of cell-surface iron transferrin receptors by cellular density and state of activation. *J. Supramol. Struct.* **1979**, *11*, 579–586.

(9) Chaston, T. B.; Lovejoy, D. B.; Watts, R. N.; Richardson, D. R. Examination of the antiproliferative activity of iron chelators: Multiple cellular targets and the different mechanism of action of triapine compared with desferrioxamine and the potent pyridoxal isonicotinoyl hydrazone analogue 311. *Clin. Cancer Res.* **2003**, *9*, 402–414.

(10) Cooper, C. E.; Lynagh, G. R.; Hoyes, K. P.; Hider, R. C.; Cammack, R.; Porter, J. B. The relationship of intracellular iron chelation to the inhibition and regeneration of human ribonucleotide reductase. *J. Biol. Chem.* **1996**, *271*, 20291–20299.

(11) Nyholm, S.; Mann, G. J.; Johansson, A. G.; Bergeron, R. J.; Graslund, A.; Thelander, L. Role of ribonucleotide reductase in inhibition of mammalian-cell growth by potent iron chelators. *J. Biol. Chem.* **1993**, *268*, 26200–26205.

(12) Fu, D.; Richardson, D. R. Iron chelation and regulation of the cell cycle: 2 mechanisms of posttranscriptional regulation of the universal cyclin-dependent kinase inhibitor p21(CIP1/WAF1) by iron depletion. *Blood* **2007**, *110*, 752–761.

(13) Le, N. T. V.; Richardson, D. R. Iron chelators with high antiproliferative activity up-regulate the expression of a growth inhibitory and metastasis suppressor gene: a link between iron metabolism and proliferation. *Blood* **2004**, *104*, 2967–2975.

(14) Nurtjahja-Tjendraputra, E.; Fu, D.; Phang, J. M.; Richardson, D. R. Iron chelation regulates cyclin D1 expression via the proteasome: A link to iron deficiency-mediated growth suppression. *Blood* **2007**, *109*, 4045–4054.

(15) Yu, Y.; Kalinowski, D. S.; Kovacevic, Z.; Siafakas, A. R.; Jansson, P. J.; Stefani, C.; Lovejoy, D. B.; Sharpe, P. C.; Bernhardt, P. V.; Richardson, D. R. Thiosemicarbazones from the old to new: Iron

chelators that are more than just ribonucleotide reductase inhibitors. *J. Med. Chem.* **2009**, *52*, 5271–5294.

(16) Kalinowski, D. S.; Richardson, D. R. The evolution of iron chelators for the treatment of iron overload disease and cancer. *Pharmacol. Rev.* **2005**, *57*, 547–583.

(17) Barnham, K. J.; Masters, C. L.; Bush, A. I. Neurodegenerative diseases and oxidative stress. *Nature Rev. Drug Discovery* **2004**, *3*, 205–214.

(18) Yuan, J.; Lovejoy, D. B.; Richardson, D. R. Novel di-2-pyridyl-derived iron chelators with marked and selective antitumor activity: In vitro and in vivo assessment. *Blood* **2004**, *104*, 1450–1458.

(19) Halliwell, B.; Gutteridge, J. M. C. Oxygen free-radicals and iron in relation to biology and medicine—Some problems and concepts. *Arch. Biochem. Biophys.* **1986**, *246*, 501–514.

(20) Chaston, T. B.; Watts, R. N.; Yuan, J.; Richardson, D. R. Potent antitumor activity of novel iron chelators derived from di-2-pyridylketone isonicotinoyl hydrazone involves fenton-derived free radical generation. *Clin. Cancer Res.* **2004**, *10*, 7365–7374.

(21) Blatt, J.; Stitely, S. Antineuroblastoma activity of desferoxamine in human cell-lines. *Cancer Res.* **1987**, *47*, 1749–1750.

(22) Donfrancesco, A.; Deb, G.; Dominici, C.; Angioni, A.; Caniglia, M.; Desio, L.; Fidani, P.; Amici, A.; Helson, L. Deferoxamine, cyclophosphamide, etoposide, carboplatin, and thiotepa (D-CECAT)—A new cytoreductive chelation-chemotherapy regimen in patients with advanced neuroblastoma. *Am. J. Clin. Oncol.-Cancer Clin. Trials* **1992**, *15*, 319–322.

(23) Donfrancesco, A.; Deb, G.; Dominici, C.; Pileggi, D.; Castello, M. A.; Helson, L. Effects of a single course of deferoxamine in neuroblastoma patients. *Cancer Res.* **1990**, *50*, 4929–4930.

(24) Estrov, Z.; Tawa, A.; Wang, X. H.; Dube, I. D.; Sulh, H.; Cohen, A.; Gelfand, E. W.; Freedman, M. H. In vitro and in vivo effects of deferoxamine in neonatal acute-leukemia. *Blood* **1987**, *69*, 757–761.

(25) Aouad, F.; Florence, A.; Zhang, Y.; Collins, F.; Henry, C.; Ward, R. J.; Crichton, R. R. Evaluation of new iron chelators and their therapeutic potential. *Inorg. Chim. Acta* **2002**, *339*, 470–480.

(26) Richardson, D. R. Molecular mechanisms of iron uptake by cells and the use of iron chelators for the treatment of cancer. *Curr. Med. Chem.* **2005**, *12*, 2711–2729.

(27) Karp, J. E.; Giles, F. J.; Gojo, L.; Morris, L.; Greer, J.; Johnson, B.; Thein, M.; Sznol, M.; Low, J. A phase I study of the novel ribonucleotide reductase inhibitor 3-aminopyridine-2-carboxaldehyde thiosemicarbazone (3-AP, Triapine(R)) in combination with the nucleoside analog fludarabine for patients with refractory acute leukemias and aggressive myeloproliferative disorders. *Leuk. Res.* **2008**, *32*, 71–77.

(28) Ma, B.; Goh, B. C.; Tan, E. H.; Lam, K. C.; Soo, R.; Leong, S. S.; Wang, L. Z.; Mo, F.; Chan, A. T. C.; Zee, B.; Mok, T. A multicenter phase II trial of 3-aminopyridine-2-carboxaldehyde thiosemicarbazone (3-AP, Triapine (R)) and gemcitabine in advanced non-small-cell lung cancer with pharmacokinetic evaluation using peripheral blood mononuclear cells. *Invest. New Drugs* **2008**, *26*, 169–173.

(29) Mackenzie, M. J.; Saltman, D.; Hirte, H.; Low, J.; Johnson, C.; Pond, G.; Moore, M. J. A Phase II study of 3-aminopyridine-2-carboxaldehyde thiosemicarbazone (3-AP) and gemcitabine in advanced pancreatic carcinoma. A trial of the Princess Margaret Hospital Phase II consortium. *Invest. New Drugs* **2007**, *25*, 553–558.

(30) Whitnall, M.; Howard, J.; Ponka, P.; Richardson, D. R. A class of iron chelators with a wide spectrum of potent antitumor activity that overcomes resistance to chemotherapeutics. *Proc. Natl. Acad. Sci. U.S.A.* **2006**, *103*, 14901–14906.

(31) Richardson, D. R.; Sharpe, P. C.; Lovejoy, D. B.; Senaratne, D.; Kalinowski, D. S.; Islam, M.; Bernhardt, P. V. Dipyridyl thiosemicarbazone chelators with potent and selective antitumor activity form iron complexes with redox activity. *J. Med. Chem.* **2006**, *49*, 6510–6521.

(32) Kalinowski, D. S.; Richardson, D. R. Future of toxicology-iron chelators and differing modes of action and toxicity: The changing face of iron chelation therapy. *Chem. Res. Toxicol.* **2007**, *20*, 715–720.

(33) Kalinowski, D. S.; Yu, Y.; Sharpe, P. C.; Islam, M.; Liao, Y. T.; Lovejoy, D. B.; Kumar, N.; Bernhardt, P. V.; Richardson, D. R. Design, synthesis, and characterization of novel iron chelators: Structure-activity relationships of the 2-benzoylpyridine thiosemicarbazone series and their 3-nitrobenzoyl analogues as potent antitumor agents. *J. Med. Chem.* **2007**, *50*, 3716–3729.

(34) Yu, Y.; Suryo Rahmanto, Y.; Richardson, D. R. Bp44mT: An orally-active iron chelator of the thiosemicarbazone class with potent anti-tumor efficacy. *Br. J. Pharmacol.* **2011**, June 9. DOI: 10.1111/j.1476-5381.2011.01526.x. [Epub ahead of print] PMID:21658021.

(35) Bernhardt, P. V.; Caldwell, L. M.; Chaston, T. B.; Chin, P.; Richardson, D. R. Cytotoxic iron chelators: Characterization of the structure, solution chemistry and redox activity of ligands and iron complexes of the di-2-pyridyl ketone isonicotinoyl hydrazone (HPKIH) analogues. *J. Biol. Inorg. Chem.* **2003**, *8*, 866–880.

(36) Richardson, D. R.; Kalinowski, D. S.; Richardson, V.; Sharpe, P. C.; Lovejoy, D. B.; Islam, M.; Bernhardt, P. V. 2-Acetylpyridine thiosemicarbazones are potent iron chelators and antiproliferative agents: Redox activity, iron complexation and characterization of their antitumor activity. *J. Med. Chem.* **2009**, *52*, 1459–1470.

(37) Richardson, D. R.; Tran, E. H.; Ponka, P. The potential of iron chelators of the pyridoxal isonicotinoyl hydrazone class as effective antiproliferative agents. *Blood* **1995**, *86*, 4295–4306.

(38) Ponka, P.; Richardson, D. R.; Edward, J. T.; Chubb, F. L. Iron chelators of the pyridoxal isonicotinoyl hydrazone class. Relationship of the lipophilicity of the apochelator to its ability to mobilize iron from reticulocytes in vitro. *Can. J. Physiol. Pharmacol.* **1994**, *72*, 659–666.

(39) Richardson, D. R.; Ponka, P. The iron-metabolism of the human neuroblastoma cell - Lack of relationship between the efficacy of iron chelation and the inhibition of DNA-synthesis. *J. Lab. Clin. Med.* **1994**, *124*, 660–671.

(40) Chaston, T. B.; Richardson, D. R. Interactions of the pyridine-2-carboxaldehyde isonicotinoyl hydrazone class of chelators with iron and DNA: Implications for toxicity in the treatment of iron overload disease. *J. Biol. Inorg. Chem.* **2003**, *8*, 427–438.

(41) Myhre, O.; Andersen, J. M.; Aarnes, H.; Fonnum, F. Evaluation of the probes 2′,7′-dichlorofluorescin diacetate, luminol, and lucigenin as indicators of reactive species formation. *Biochem. Pharmacol.* **2003**, *65*, 1575–1582.

(42) Ghose, A. K.; Crippen, G. M. Atomic physicochemical parameters for 3-dimensional-structure-directed quantitative structure-activity-relationships. 2. Modeling dispersive and hydrophobic interactions. *J. Chem. Inf. Comput. Sci.* **1987**, *27*, 21–35.

(43) Sheldrick, G. M. A short history of SHELX. *Acta Crystallogr., Sect. A* **2008**, *64*, 112–122.

(44) Farrugia, L. J. ORTEP-3 for windows—A version of ORTEP-III with a graphical user interface (GUI). *J. Appl. Crystallogr.* **1997**, *30*, 565.

(45) Farrugia, L. J. WinGX suite for small-molecule single-crystal crystallography. *J. Appl. Crystallogr.* **1999**, *32*, 837–838.

(46) Richardson, D. R.; Milnes, K. The potential of iron chelators of the pyridoxal isonicotinoyl hydrazone class as effective antiproliferative agents 0.2. The mechanism of action of ligands derived from salicylaldehyde benzoyl hydrazone and 2-hydroxy-1-naphthylaldehyde benzoyl hydrazone. *Blood* **1997**, *89*, 3025–3038.

(47) Baker, E.; Richardson, D.; Gross, S.; Ponka, P. Evaluation of the iron chelation potential of hydrazones of pyridoxal, salicylaldehyde and 2-hydroxy-1-naphthylaldehyde using the hepatocyte in culture. *Hepatology* **1992**, *15*, 492–501.

(48) Becker, E.; Richardson, D. R. Development of novel aroylhydrazone ligands for iron chelation therapy: 2-Pyridylcarboxaldehyde isonicotinoyl hydrazone analogs. *J. Lab. Clin. Med.* **1999**, *134*, 510–521.

(49) Richardson, D. R.; Baker, E. The uptake of iron and transferrin by the human-malignant melanoma cell. *Biochim. Biophys. Acta* **1990**, *1053*, 1–12.

(50) Richardson, D. R.; Baker, E. Intermediate steps in cellular iron uptake from transferrin - Detection of a cytoplasmic pool of iron, free of transferrin. *J. Biol. Chem.* **1992**, *267*, 21384–21389.

(51) Dean, R. T.; Nicholson, P. The action of 9 chelators on iron-dependent radical damage. *Free Radical Res.* **1994**, *20*, 83–101.